Fig. 5

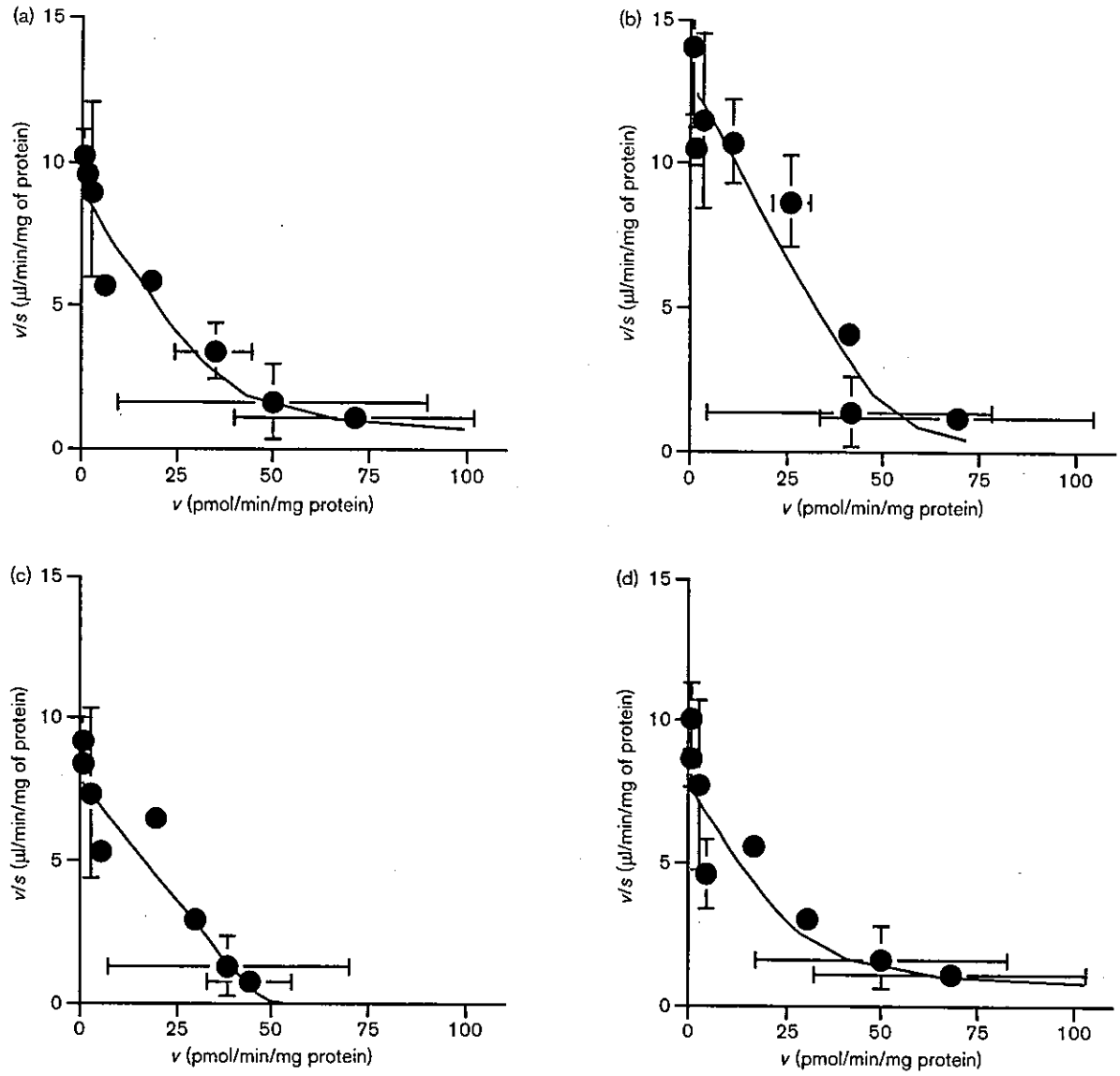

Eadie–Hofstee plot for OATP1B1-mediated uptake of [^{3}H] $E_2$17βG. The transport velocity determined by examining the uptake of [^{3}H] $E_2$17βG for 2 min was determined in OATP1B1*1a (a), OATP1B1*1b (b), OATP1B1*5 (c), and OATP1B1*15 (d) expressing HEK293 cells. Each point and bar represents the mean ± SE of three independent experiments. The solid line represents the fitted line. The OATP1B1 mediated transports were obtained by subtracting the transport velocity in vector-transfected cells from those in OATP1B1 SNP variants-expressed cells.

Table 1 Kinetic parameters for the transport of [^{3}H] $E_2$17βG

Genotype	K_m (μM)	V_{max} (pmol/min/mg protein)	P_{dif} (μl/min/mg protein)	V_{max}/K_m (μl/min/mg protein)	Expression amount (% of *1a)	Corrected V_{max} (% of *1a)
OATP1B1*1a	4.3 ± 1.7	35.7 ± 12.9	0.644 ± 0.306	8.38 ± 4.46	100	100
OATP1B1*1b	4 ± 1.3	49.3 ± 14.9	0.222 ± 0.344	12.4 ± 5.5	130	110
OATP1B1*5	5.9 ± 2.0	46.6 ± 15.1	0.015 ± 0.2762	7.9 ± 3.7	140	93
OATP1B1*15	4.07 ± 2.5	28.8 ± 16.1	0.738 ± 0.399	7.06 ± 5.84	1100	7.3

Data shown in Fig. 5 were analyzed to determine the kinetic parameters. Moreover, the V_{max} values were normalized by the expression level of OATP1B1 protein determined by the Western blot analysis shown in Fig. 3.

Fig. 6

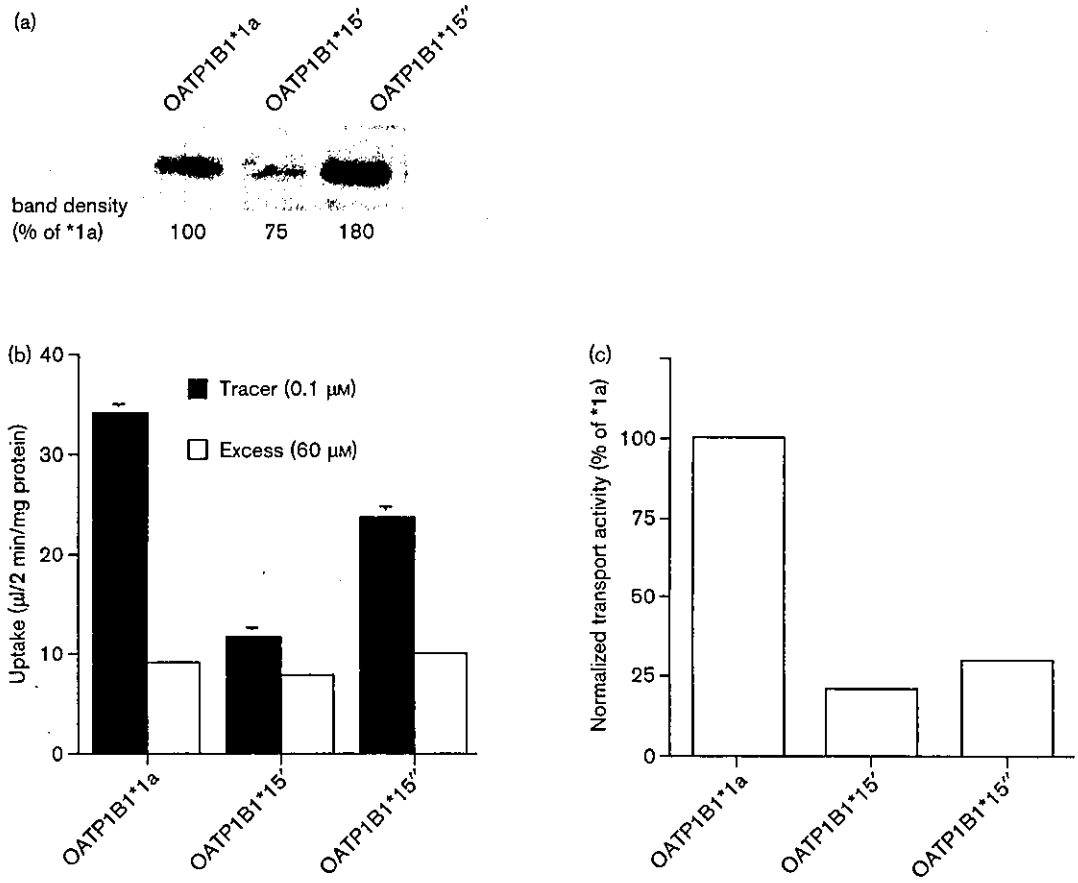

Western blot analysis and uptake study using other OATP1B1*15 clones. The uptake of $E_2$17βG was examined using other two OATP1B1*15 clones. The expression level of OATP1B1 was also determined by the Western blot analysis. (a) Crude membrane (10 μg) obtained from HEK293 cells was separated by SDS–PAGE (7%). OATP1B1 proteins were detected using horseradish peroxidase-labeled anti-rabbit IgG after incubation with the polyclonal antibody for OATP1B1. (b) HEK293 cells expressing OATP1B1*1a, OATP1B1*15 clones 1 and 2 were incubated for 2 min in the presence of [^{3}H] $E_2$17βG with tracer (0.1 μM; closed bar) or excess (60 μM; open bar) concentration of unlabeled $E_2$17βG. Each point and bar represents the mean ± SE of three independent experiments. (c) The transport activity was obtained by subtracting the transport velocity in the presence of excess amount of unlabeled $E_2$17βG from the transport velocity in its absence shown in (b). Then, the normalized transport activity was calculated by normalizing the transport activity by the OATP1B1 expression level estimated from (a).

mediated uptake of this drug due to the low transport activity compared with the background level. This result is consistent with our previous transcellular transport studies with MDCK II monolayer expressing the uptake (OATP1B1) and efflux (MRP2) transporters on the basolateral and apical membrane, respectively; the extent of the basal-to-apical transport of pravastatin was less than 20% of that of $E_2$17βG [16]. It is unfortunate that the transport of pravastatin was not detectable under the present experimental conditions. However, our previous in-vivo findings that the non-renal clearance of pravastatin is much lower in OATP1B1*15 subjects [15] is consistent with the reduced transport function of OATP1B1*15 determined in the present study.

Focusing on the OATP1B1*5 allele, two groups have reported contradictory results. Nozawa *et al.* [14] demonstrated that the localization and transport activity of OATP1B1*5 was similar to that of OATP1-B1*1a using HEK293 as host cells, which is consistent with the present results (Fig. 1). In contrast, Tirona *et al.* [13] used HeLa cells and observed a reduction in the cell surface expression of OATP1B1*5. This discrepancy may be due to a difference in the membrane targeting mechanism between HEK293 and HeLa cells. Although we also found the membrane localization of OATP1B1*15 in our HEK 293 cells, we need to be careful in expecting in-vivo cellular localization from the results of in-vitro expression system. Indeed, the difference in the cellular localization of transporters was reported previously [20–23]. It is also difficult for us to determine the in-vivo function of OATP1B1*5 from

the drug disposition due to the low frequency of OATP1B1*5 in Japanese subjects.

Finally, the expression level of SNP variants of OATP1B1 needs to be discussed. The expression level of the OATP1B1*15 clone analyzed in the present study was 11 times higher than that of OATP1B1*1a. In order to demonstrate that this high expression is not a unique characteristic of OATP1B1*15 and to confirm that the transport function of OATP1B1*15 is indeed reduced compared with the wild-type OATP1B1, we determined the expression level and transport properties of OATP1B1*15 in other clones, which were picked up during the selection in the presence of zeocin. The OATP1B1*15 expression level in two other clones was 75 and 180% that of OATP1B1*1a, indicating that high expression is not necessarily associated with the OATP1B1*15 variation (Fig. 6). In addition, their intrinsic transport activity for $E_2$17βG was also reduced to 21 and 30% of OATP1B1*1a (Fig. 6), after correction of their protein expression levels. Using these two clones, it was confirmed that the transport function is indeed reduced in OATP1B1*15.

In conclusion, we analyzed the function of four OATP1B1 SNPs variants. Although all the SNP variants examined in the present study were located on the cellular membrane, the intrinsic V_{max} value for $E_2$17βG in the OATP1B1*15 variant was reduced to 7.3% that in OATP1B1*1a. The degree of the reduction in V_{max} is similar to that for the non-renal clearance of pravastatin in healthy Japanese subjects with the OATP1B1*15 allele [15]. These results suggest that in-vitro transport experiments with cDNA-transfected HEK293 cells are useful tools for predicting the effects of OATP1B1 SNPs on in-vivo drug disposition.

References

1 Evans WE and Relling MV. Pharmacogenomics: translating functional genomics into rational therapeutics. *Science* 1999; **286**:487–491.
2 Evans WE and McLeod HL. Pharmacogenomics – drug disposition, drug targets, and side effects. *N Engl J Med* 2003; **348**:538–549.
3 Meyer UA and Zanger UM. Molecular mechanisms of genetic polymorphisms of drug metabolism. *Annu Rev Pharmacol Toxicol* 1997; **37**: 269–296.
4 Rodrigues AD and Rushmore TH. Cytochrome P450 pharmacogenetics in drug development: in vitro studies and clinical consequences. *Curr Drug Metab* 2002; 3:289–309.
5 Hoffmeyer S, Burk O, von Richter O, Arnold HP, Brockmoller J, Johne A, *et al.* Functional polymorphisms of the human multidrug-resistance gene: multiple sequence variations and correlation of one allele with P-glycoprotein expression and activity in vivo. *Proc Natl Acad Sci U S A* 2000; **97**:3473–3478.
6 Hsiang B, Zhu Y, Wang Z, Wu Y, Sasseville V, Yang WP, *et al.* A novel human hepatic organic anion transporting polypeptide (OATP2). Identification of a liver-specific human organic anion transporting polypeptide and identification of rat and human hydroxymethylglutaryl-CoA reductase inhibitor transporters. *J Biol Chem* 1999; **274**:37161–37168.
7 Konig J, Cui Y, Nies AT, Keppler D. A novel human organic anion transporting polypeptide localized to the basolateral hepatocyte membrane. *Am J Physiol Gastrointest Liver Physiol* 2000; **278**:G156–G164.
8 Tamai I, Nezu J, Uchino H, Sai Y, Oku A, Shimane M, *et al.* Molecular identification and characterization of novel members of the human organic anion transporter (OATP) family. *Biochem Biophys Res Commun* 2000; **273**:251–260.
9 Abe T, Kakyo M, Tokui T, Nakagomi R, Nishio T, Nakai D, *et al.* Identification of a novel gene family encoding human liver-specific organic anion transporter LST-1. *J Biol Chem* 1999; **274**:17159–17163.
10 Cui Y, Konig J, Leier I, Buchholz U, Keppler D. Hepatic uptake of bilirubin and its conjugates by the human organic anion transporter SLC21A6. *J Biol Chem* 2001; **276**:9626–9630.
11 Tamai I, Nozawa T, Koshida M, Nezu J, Sai Y, Tsuji A. Functional characterization of human organic anion transporting polypeptide B (OATP-B) in comparison with liver-specific OATP-C. *Pharm Res* 2001; **18**:1262–1269.
12 Michalski C, Cui Y, Nies AT, Nuessler AK, Neuhaus P, Zanger UM, *et al.* A naturally occurring mutation in the SLC21A6 gene causing impaired membrane localization of the hepatocyte uptake transporter. *J Biol Chem* 2002; **277**:43058–43063.
13 Tirona RG, Leake BF, Merino G, Kim RB. Polymorphisms in OATP-C: identification of multiple allelic variants associated with altered transport activity among European- and African-Americans. *J Biol Chem* 2001; **276**:35669–35675.
14 Nozawa T, Nakajima M, Tamai I, Noda K, Nezu J, Sai Y, *et al.* Genetic polymorphisms of human organic anion transporters OATP-C (SLC21A6) and OATP-B (SLC21A9): allele frequencies in the Japanese population and functional analysis. *J Pharmacol Exp Ther* 2002; **302**:804–813.
15 Nishizato Y, Ieiri I, Suzuki H, Kimura M, Kawabata K, Hirota T, *et al.* Polymorphisms of OATP-C (SLC21A6) and OAT3 (SLC22A8) genes: consequences for pravastatin pharmacokinetics. *Clin Pharmacol Ther* 2003; **73**:554–565.
16 Sasaki M, Suzuki H, Ito K, Abe T, Sugiyama Y. Transcellular transport of organic anions across a double-transfected Madin–Darby canine kidney II cell monolayer expressing both human organic anion-transporting polypeptide (OATP2/SLC21A6) and Multidrug resistance-associated protein 2 (MRP2/ABCC2). *J Biol Chem* 2002; **277**:6497–6503.
17 Ogawa K, Suzuki H, Hirohashi T, Ishikawa T, Meier PJ, Hirose K, *et al.* Characterization of inducible nature of MRP3 in rat liver. *Am J Physiol Gastrointest Liver Physiol* 2000; **278**:G438–G446.
18 Sugiyama D, Kusuhara H, Shitara Y, Abe T, Meier PJ, Sekine T *et al.* Characterization of the efflux transport of 17β-D-17β-glucuronide from the brain across the blood-brain barrier. *J Pharmacol Exp Ther* 2001; **298**:316–322.
19 Yamaoka K, Tanigawara Y, Nakagawa T, Uno T. A pharmacokinetic analysis program (multi) for microcomputer. *J Pharmacobiodyn* 1981; **4**:879–885.
20 Masuda S, Saito H, Inui KI. Interactions of nonsteroidal anti-inflammatory drugs with rat renal organic anion transporter, OAT-K1. *J Pharmacol Exp Ther* 1997; **283**:1039–1042.
21 Masuda S, Ibaramoto K, Takeuchi A, Saito H, Hashimoto Y, Inui KI. Cloning and functional characterization of a new multispecific organic anion transporter, OAT-K2, in rat kidney. *Mol Pharmacol* 1999; **55**: 743–752.
22 Gu HH, Ahn J, Caplan MJ, Blakely RD, Levey AI, Rudnick G. Cell-specific sorting of biogenic amine transporters expressed in epithelial cells. *J Biol Chem* 1996; **271**:18100–18106.
23 Folsch H, Ohno H, Bonifacino JS, Mellman I. A novel clathrin adaptor complex mediates basolateral targeting in polarized epithelial cells. *Cell* 1999; **99**:189–198.

Pharmaceutical Research, Vol. 21, No. 10, October 2004 (© 2004)

Research Paper

Functional Analysis of SNPs Variants of BCRP/ABCG2

Chihiro Kondo,[1] Hiroshi Suzuki,[2] Masaya Itoda,[3] Shogo Ozawa,[3] Jun-ichi Sawada,[3] Daisuke Kobayashi,[4] Ichiro Ieiri,[5] Kazunori Mine,[4] Kenji Ohtsubo,[5] and Yuichi Sugiyama[1,6]

Received February 27, 2004; accepted June 21, 2004

Purpose. The aim of the current study was to identify the effect of single nucleotide polymorphisms (SNPs) in breast cancer resistance protein (BCRP/ABCG2) on its localization, expression level, and transport activity.

Methods. The cellular localization was identified using the wild type and seven different SNP variants of BCRP (V12M, Q141K, A149P, R163K, Q166E, P269S, and S441N BCRP) after transfection of their cDNAs in plasmid vector to LLC-PK1 cells. Their expression levels and transport activities were determined using the membrane vesicles from HEK293 cells infected with the recombinant adenoviruses containing these kinds of BCRP cDNAs.

Results. Wild type and six different SNP variants of BCRP other than S441N BCRP were expressed on the apical membrane, whereas S441N BCRP showed intracellular localization. The expression levels of Q141K and S441N BCRP proteins were significantly lower compared with the wild type and the other five variants. Furthermore, the transport activity of E_1S, DHEAS, MTX, and PAH normalized by the expression level of BCRP protein was almost the same for the wild type, V12M, Q141K, A149P, R163K, Q166E, and P269S BCRP.

Conclusions. These results suggest that Q141K SNPs may associate with a lower expression level, and S441N SNPs may affect both the expression level and cellular localization. It is possible that subjects with these polymorphisms may have lower expression level of BCRP protein and, consequently, a reduced ability to export these substrates.

KEY WORDS: adenovirus; BCRP/ABCG2; interindividual difference; SNPs.

INTRODUCTION

ABCG2, also referred to as breast cancer resistance protein (BCRP), mitoxantrone resistance-associated protein (MXR), and placenta-specific ATP-binding cassette transporter (ABCP), is a member of the ATP-binding cassette (ABC) transmembrane transporter family (1–3). BCRP mRNA encodes a 72.6 kDa membrane protein composed of 655 amino acids (1,3,4). It has a single ATP binding domain at the amino terminus (at amino acid 61-270) followed by six transmembrane domains (at amino acids 394-416, 428-450, 478-499, 506-528, 533-555 and 629-651) (1,5). BCRP may form a homodimer to become functionally active (6). In BCRP-expressing cells, the intracellular concentration of substrate anticancer drugs is reduced, suggesting its protective role against drug toxicity (7). In normal human tissues, BCRP is expressed on the apical membrane of enterocytes, trophoblast cells in the placenta, the bile canalicular membrane of hepatocytes, and the apical membrane of lactiferous ducts in the mammary gland (8). Current evidence indicates that BCRP could contribute to the disposition of some substrates (9,10). Moreover, it was recently shown that BCRP also transports some endogenous compounds such as sulfate conjugates (11). It is also reported that some mutations in the open reading frame of BCRP are associated with resistance to some anticancer drugs. For example, an amino acid mutation at position 482 affects the resistance to adriamycin and methotrexate (12,13). Therefore, it is possible that certain kinds of single nucleotide polymorphisms (SNPs) of BCRP may alter its function and, consequently, affect the disposition of substrate drugs.

To date, some pieces of information about BCRP SNPs have been reported. Recently, the SNPs of BCRP in 100 healthy Japanese subjects have been analyzed in 84 cell lines established from clinically dissected human tumors and also in 60 Japanese individuals who were given irinotecan, an anticancer drug, for the treatment of various types of cancer (14). On analyzing the specimens from the 100 Japanese volunteers, 7 kinds of SNPs were identified for the BCRP gene: G34A (V12M), C376T (Q376Stop), C421A (Q141K), G1098A (E366E), G1322A (S441N), T1465C (F489L), and C1515- (AFFVM505-509ASSL Stop). The allele frequencies of these SNPs are 18, 1, 36, 1, 0.5, 0.5, and 0.5%, respectively. In the 84 cell lines, 7 kinds of SNPs were identified and their frequency for G34A (V12M), C376T (Q126Stop), C421A (Q141K), G445C (A149P), G488A (R163K), C805T (P269S), and G1098A (E366E) are 22, 3, 29, 1, 0.6, 0.6 and 2%, respectively. In the present study, we focused on the 7 SNPs, 6 of which were found in Japanese samples and cell samples, and 1 was reported in the NCBI database (rs1061017). We constructed expression systems for the wild type and SNPs variants of BCRP (V12M, Q141K, A149P, R163K, Q166E, P269S, S441N BCRP) and examined whether these SNPs variants of BCRP alter its localization, expression level, and transport activity.

MATERIALS AND METHODS

Materials

[^{3}H]Estrone-3-sulfate (E_1S; 46 Ci/mmol), [^{3}H]dehydroepiandrosterone sulfate (DHEAS; 79.1 Ci/mmol), and [^{3}H]*p*-aminohippuric acid (PAH; 4.51 Ci/mmol) were purchased from PerkinElmer Life Science, Inc. (Boston, MA, USA). [^{3}H]Methotrexate (29 Ci/mmol) was purchased from Ameri-

[1] School of Pharmaceutical Sciences, The University of Tokyo, Hongo, Bunkyo-ku, Tokyo 113-0033, Japan.
[2] Department of Pharmacy, Tokyo University Hospital, The University of Tokyo, Hongo, Bunkyo-ku, Tokyo 113-0033, Japan.
[3] National Institute of Health Sciences, Kamiyoga, Setagaya-ku, Tokyo 158-8501, Japan.
[4] School of Pharmaceutical Sciences, Kyushu University, Maidashi, Higashi-ku, Fukuoka 812-8582, Japan.
[5] Department of Hospital Pharmacy, Faculty of Medicine, Tottori University, Yonago, Tottori, 683-8504, Japan.
[6] To whom correspondence should be addressed. (e-mail: sugiyama@mol.f.u-tokyo.ac.jp)

ABBREVIATIONS: ABC transporter, ATP-binding cassette transmembrane transporter; Ad, adenovirus; BCRP, breast cancer resistance protein; DHEAS, dehydroepiandrosterone sulfate; E_1S, estrone 3-sulfate; ER, endoplasmic reticulum; K_m, Michaelis constant; MOI, multiplicity of infection; MTX, methotrexate; PAH, *p*-aminohippurate; SNPs, single nucleotide polymorphisms; V_{max}, maximum transport velocity.

can Radiolabeled Chemicals, INC. (St. Louis, MO, USA). Unlabeled E_1S, DHEAS, methotrexate, PAH, and ATP, creatine phosphate, and creatine phosphokinase were purchased from Sigma Chemical (St. Louis, MO, USA). All other chemicals used were commercially available and of reagent grade.

LLC-PK1 and HEK293 cells were cultured in Medium 199 (GIBCO BRL, Gaithersburg, MD, USA) and Dulbecco's modified Eagle's medium (GIBCO BRL), respectively, after addition of 10% fetal bovine serum, and penicillin (100 U/ml) and streptomycin (100 mg/ml).

Construction of BCRP-Containing Expression Vectors and Recombinant Adenovirus

Wild-type BCRP cDNA was purchased from Invitrogen Corp. (Carlsbad, CA, USA) (no. H24176). The complete BCRP cDNA was amplified with the primers containing NheI site and Kozak sequence attached at the 5'-end and that with the ApaI site at the 3'-end by PCR, and then was inserted into pcDNA3.1 vector plasmid, resulting in wt BCRP/pcDNA3.1. Using site-directed mutagenesis, SNP variants of BCRP (V12M, Q141K, A149P, R163K, Q166E, P269S and S441N BCRP) were constructed on pcDNA3.1 vector (SNPs type BCRP/pcDNA3.1). V12M BCRP was amplified with 5'-GTCGAAGTTTTTATCCCAATGTCACAAGGAAACACCAATGGC-3' and '-GCCATTGGTGTTTCCTTGTGACATTGGGATAAAAACTTCGAC-3'. Q141K BCRP was amplified with 5'-CGGTGAGAGAAAACTTAAAGTTCTCAGCAG-3' and '-GCTGCTGAGAACTTTAAGTTTTCTCTCACCG-3'. A149P BCRP was amplified with 5'-GCAGCTCTTCGGCTTCCAACAACTATGACG-3' and '-CGTCATAGTTGTTGGAAGCCGAAGAGCTGC-3'. R163K BCRP was amplified with 5'-CGAACGGATTAACAAGGTCATTCAAGAG-3' and 5'-CTCTTGAATGACCTTGTTAATCCGTTCG-3'. Q166E BCRP was amplified with 5'-GATTAACAGGGTCATTGAAGAGTTAGGTCT-3' and 5'-CCAGACCTAACTCTTCAATGACCCTGTTAA-3'. P269S BCRP was amplified with 5'-GACTTATGTTCCACGGGTCTGCTCAGGAGGCCTTGGG-3' and 5'-CCCAAGGCCTCCTGAGCAGACCCGTGGAACATAAGTC-3'. S441N BCRP was amplified with 5'-CCAACCAGTGTTTCAGCAATGTTTCAGCCGTGGAACTC-3' and 5'-GAGTTCCACGGCTGAAACATTGCTGAAACACTGGTTGG-3'. From these pcDNA3.1 vectors, BCRP cDNA was subcloned into the NheI and ApaI sites of the pShuttle plasmid vector, transferred into Adeno-XTM Viral DNA using the Adeno-X Expression System (BD Biosciences, Palo Alto, CA, USA), resulting in pAd-wt BCRP. To produce recombinant adenovirus, pAd-wt BCRP was digested with PacI, and transfected to HEK293 cells by FuGENE6 (Roche Diagnostics Corporation, Indianapolis, IN, USA) according to the manufacturer's instructions. For SNPs type BCRPs, viruses were prepared in the same way, resulting in the production of pAd-SNPs BCRP (pAd-V12M, Q141K, A149P, R163K, Q166E, P269S, and S441N BCRP). Recombinant viruses prepared as described previously (Ad-wt BCRP and Ad-SNPs type BCRP) (15) were purified by CsCl gradient centrifugation, dialyzed with a solution containing 10 mM Tris (pH 7.5), 1 mM $MgCl_2$, and 10% glycerol, and stored in aliquots at -80°C. Then, the resulting virus titer was determined as described previously (16).

Immunohistochemical Staining

For immunohistochemical staining, LLC-PK1 cells transfected with wild-type BCRP or SNPs type BCRP in pcDNA3.1 vector were plated at a density of 5×10^5 cells in 12-well dishes, 72 h prior to the experiments. After fixation with 4% (w/v) paraformaldehyde for 10 min and permeabilization in 1% TritonX-100 in PBS for 10 min, cells were incubated with the monoclonal antibody against BCRP (BXP-21) (Kamiya Biomedical Company, Seattle, WA, USA) for 1 h at room temperature. Then, cells were washed three times with PBS and incubated with Goat anti-mouse IgG Alexa 488 (Molecular Probes, Inc., Eugene, OR, USA) diluted 250-fold in PBS for 1 h at room temperature, and mounted in VECTASHIELD Mounitng Medium (Vector Laboratories, Burlingame, CA, USA). The localization of BCRP protein was visualized by confocal lazer microscopy (Zeiss LSM-510; Carl Zeiss Inc., Thornwood, NY, USA).

Preparation of Membrane Vesicles

To prepare membrane vesicles, HEK293 cells were plated at a density of 2×10^6 cells per 15 cm dish. After 72 h, cells were infected with recombinant adenoviruses containing the wild-type and SNPs type BCRP at 2×10^7 pfu per plate. As a negative control, cells were infected with the virus containing GFP cDNA (pAd-GFP). Cells were harvested at 48 h after infection and then the membrane vesicles were isolated using a standard method described previously in detail (17). Briefly, cells were diluted 40-fold with hypotonic buffer (1 mM Tris-HCl, 0.1 mM EDTA, pH 7.4, at 4°C) and stirred gently for 1 h on ice in the presence of 2 mM phenylmethylsulfonyl fluoride, 5 μg/ml leupeptin, 1 μg/ml pepstatin, and 5 μg/ml aprotinin. The cell lysate was centrifuged at 100,000 × *g* for 30 min at 4°C and the resulting pellet was suspended in 10 ml isotonic TS buffer (10 mM Tris-HCl, 250 mM sucrose, pH 7.4 at 4°C) and homogenized in a Dounce B homogenizer (glass/glass, tight pestle, 30 strokes). The crude membrane fraction was layered on top of a 38% (w/v) sucrose solution in 5 mM Tris-HEPES, pH 7.4 at 4°C, and centrifuged in a Beckman SW41 rotor centrifuge at 280,000 × *g* for 45 min at 4°C. The turbid layer at the interface was collected, diluted to 23 ml with TS buffer, and centrifuged at 100,000 × *g* for 30 min at 4°C. The resulting pellet was suspended in 400 μl TS buffer. Vesicles were formed by passing the suspension 30 times through a 27-gauge needle using a syringe. The membrane vesicles were finally frozen in liquid nitrogen and stored at -80°C until required. Protein concentrations were determined by the Lowry method.

Western Blot Analysis

For the Western blot analysis, membrane vesicles were dissolved in 3 x SDS sample buffer (New England BioLabs, Beverly, MA, USA), and separated on a 10% SDS-polyacrylamide gel electrophoresis plate with a 4.4% stacking gel. The molecular weight was determined using a prestained protein marker (New England BioLabs). Proteins were transferred electrophoretically to a polyvinylidene diflouride membrane (Pall, East Hills, NY, USA) using a blotter (Bio-Rad Laboratories, Richmond, CA, USA) at 15 V for 1 h The membrane was blocked with PBS containing 5% skimmed milk for 1 h at room temperature. After blocking, the membrane was incubated for 1 h at room temperature in BXP-21

(Kamiya Biomedical Company, Seattle, WA, USA) diluted 100-fold with 5% skimmed milk. Then, the membrane was washed with PBS containing 0.1% Tween-20 and allowed to bind to Alexa Fluor 680 goat anti-mouse IgG (Molecular Probes, Inc. Eugene, OR, USA) which was diluted 5,000-fold with skimmed milk for 1 h to detect BCRP. Subsequently, the fluorescence was measured in a densitometer (Odyssey, ALOKA, Tokyo, Japan). The protein expression levels of each SNPs variant of BCRP were determined by analyzing the band density associated with three different applied amount of the membrane vesicles on the Western blot analysis.

Vesicle Transport Assays

The uptake study of [^{3}H]E_1S, [^{3}H]DHEAS, [^{3}H]MTX, [^{3}H]PAH was performed as reported previously (18). Briefly, the transport medium (10 mM Tris, 250 mM sucrose and 10 mM $MgCl_2$, pH 7.4) contained the ligands, 5 mM ATP and an ATP-regenerating system (10 mM creatine phosphate and 100 mg/ l creatine phosphokinase). An aliquot of transport medium (15 μl) was mixed rapidly with the vesicle suspension (2 μg protein for [^{3}H] E_1S and 10 μg protein for others in 5 μl). The transport reaction was stopped by the addition of 1 ml ice-cold buffer containing 250 mM sucrose, 0.1 M NaCl and 10 mM Tris-HCl (pH 7.4). 900 μl of the stopped reaction mixture was passed through a 0.45 μm HA filter (Millipore Corp., Bedford, MA, USA), and then washed twice with 5 ml stop solution. The radioactivity retained on the filter was measured in a liquid scintillation counter (LS 6000SE, Beckman Instruments, Fullerton, CA, USA) after the addition of scintillation cocktail (Clear-sol I, Nacalai Tesque, Tokyo, Japan). The amount of ligand taken up into vesicles was normalized in terms of the amount of membrane protein. The uptake activity was defined as the amount of ligand divided by the ligand concentration in the medium. The ATP-dependent uptake of ligands was calculated by subtracting the ligand uptake in the absence of ATP from that in its presence.

RESULTS

Localization of Human BCRP in LLC-PK1 Cells

The localization of human BCRP was determined by immunohistochemical staining. Monoclonal antibody against human BCRP (BXP-21) detected a high fluorescence signal at the apical membrane of LLC-PK1 cells after transfection of the wild type BCRP/pc DNA3.1 (Fig. 1). No specific fluorescence signal was observed at the apical membrane or in the cytoplasm after transfection of pcDNA3.1 plasmid vector (data not shown). We also analyzed the cellular localization of BCRP variants. In our experimental system, except for one SNP variant of BCRP (S441N BCRP/pcDNA3.1), all variants showed the same localization as the wild-type BCRP, at the apical membrane of LLC-PK1 cells (Fig. 1). S441N BCRP was expressed intracellularly (Fig. 1).

Expression Level of Human BCRP in HEK293 Cells Using Recombinant Adenoviruses

The expression level of BCRP in the membrane fraction isolated from the BCRP-expressing HEK293 cells was determined by Western blot analysis using an anti-human BCRP monoclonal antibody (BXP-21). As previously reported, BCRP was detected at an approximate molecular weight of 72 kDa (Fig. 2). In contrast, in the membrane vesicles from the Ad-GFP infected cells, no BCRP was detected (Fig. 2). The expression levels of wild-type BCRP and variants were estimated from the band density. Except for two BCRP variants (Q141K and S441N BCRP), the expression levels of each BCRP SNPs were approximately the same as that of the wild-type BCRP (Fig. 2). The expression level of Q141K BCRP was approximately 30–40% of the wild-type BCRP, whereas that of S441N BCRP was much lower, and could not be determined with any accuracy (Fig. 2).

Transport Activity of BCRP

Because we previously reported that [^{3}H]E_1S is taken up into BCRP-expressing membrane vesicles in an ATP-

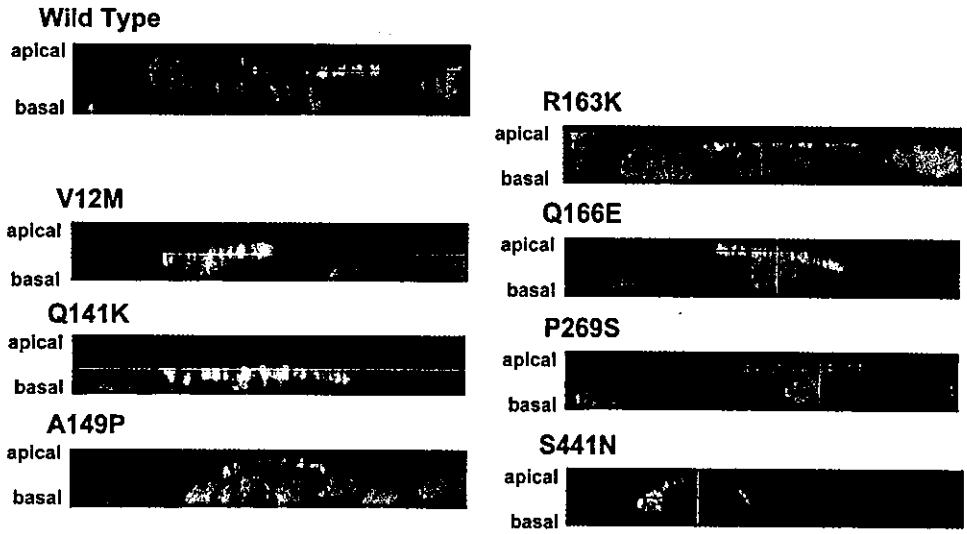

Fig. 1. Localization of BCRP in LLC-PK1 cells. The immunolocalization of BCRP molecules in the LLC-PK1 cells transfected with BCRP cDNA was determined using monoclonal antibody against BCRP (green). Nuclei were stained with PI (red). Figures show the Z-sectioning images, top side of the figure shows the apical membrane, and bottom side is the basal membrane.

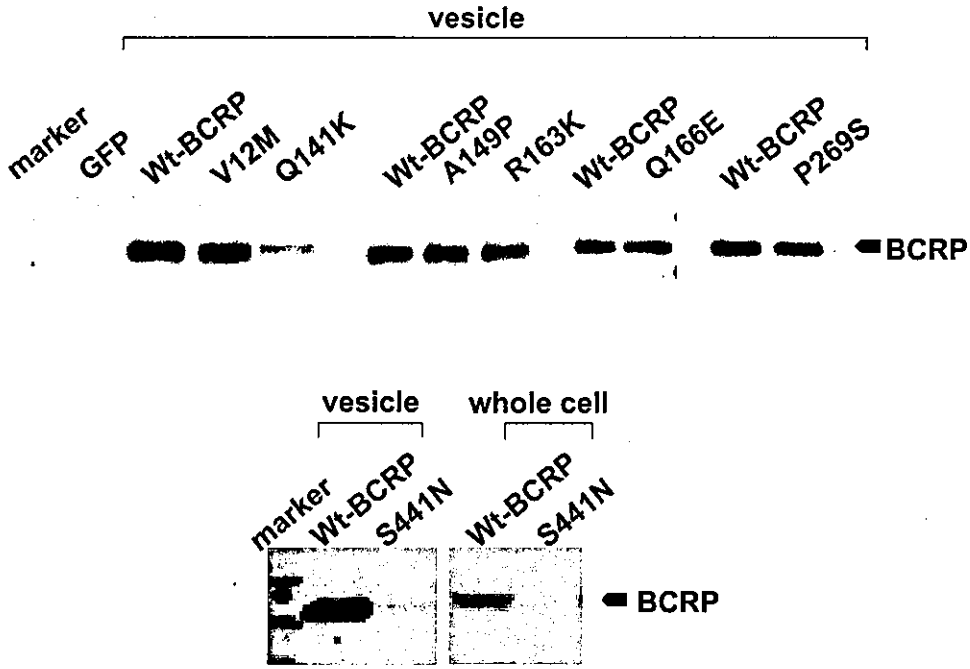

Fig. 2. Expression level of BCRP in membrane vesicles. The expression level of the wild type and SNPs variants of BCRP proteins was determined in the isolated membrane vesicles from HEK293 cells infected with recombinant adenovirus using Western blot analysis. The expression levels of wild type and S441N SNPs BCRP were also determined also in whole cell lysates.

dependent manner (11), the effect of SNPs on the BCRP-mediated transport of $[^3H]E_1S$ was examined. In the current study, we used the same batch of transfected cells for measurement of the expression level and transport activity. Ad-wt BCRP expressing membrane vesicles transported $[^3H]E_1S$ up to approximately 0.5 nmol min^{-1} mg^{-1} membrane protein, whereas no uptake of $[^3H]E_1S$ was observed by the membrane vesicles from Ad-GFP infected cells. Because the amount of $[^3H]E_1S$ molecules taken up by 2 μg membrane vesicles at 1 min (1 pmol) is approximately 1/10 of that in the incubation medium (10 pmol), $[^3H]E_1S$ molecules were not depleted from the incubation medium. Based on this consideration, it is possible for us to determine the initial uptake velocity from 1 min data. Indeed, we could find that the time profile for the BCRP-mediated uptake of $[^3H]E_1S$ was linear up to 2 min.

Except for two SNP variants of BCRP (Q141K and S441N BCRP), the ATP-dependent uptakes per mg membrane protein of SNP variants (V12M, A149P, R163K, Q166E, P269S BCRP) were similar to that of the wild-type BCRP (Fig. 3a). The uptake activity of Q141K BCRP per mg membrane protein was approximately 30–40% of the wild-type BCRP, and that of S441N was almost the same as that of the GFP-infected control cells. These uptake activities were inhibited by the excess amount of E_1S, 100 μM (Fig. 3a).

Then, in order to compare the intrinsic transport activity of the wild-type and SNP variants of BCRP, the uptake determined per mg membrane protein (Fig. 3a) was normalized relative to the expression levels estimated by Western blot analysis (Fig. 2), except for S441N BCRP the expression level of which was extremely low (Fig. 2). As shown in Fig. 3b, the transport activity of other SNP variants of BCRP (V12M, Q141K, A149P, R163K, Q166E, and P269S BCRP) was almost identical to that of the wild-type BCRP.

As far as V12M and Q141K BCRP were concerned, these have a high allele frequency in Japanese and we determined the kinetic parameters for the transport of $[^3H]E_1S$. As shown in Fig. 4, the ATP-dependent uptake of $[^3H]E_1S$ was saturable, and the K_m values were 11.6 ± 4.79, 9.07 ± 1.52, and 14.0 ± 7.27 μM, and the V_{max} values were 13.3 ± 3.3, 13.5 ± 1.29, and 4.57 ± 1.58 nmol min^{-1} mg^{-1} protein, for the wild type, V12M, and Q141K BCRP, respectively. In addition to $[^3H]E_1S$, the transport of other BCRP substrates was examined. As previously reported, ATP-dependent uptake of [^{3}H]methotrexate and [^{3}H]DHEAS was observed. The absolute values of their transport activity were about at 7.5 pmol 2 min^{-1} mg^{-1} mebrane protein and 150 pmol 2 min^{-1} mg^{-1} membrane protein, whereas GFP-expressing membrane vesicles tranport them at about 0.5 pmol 2 min^{-1} mg^{-1} membrane protein and 25 pmol 2 min^{-1} mg^{-1} membrane protein, respectively. Moreover, BCRP-mediated transport of [^{3}H]PAH was also detectable, and the activity of this was 10 pmol 2 min^{-1} mg^{-1} membrane protein, whereas GFP-expressing membrane vesicles tranport them at about 0.5 pmol 2 min^{-1} mg^{-1} membrane protein. Figure 5a shows the ATP-dependent uptake of DHEAS, PAH, and MTX per mg membrane protein for the wild-type and SNPs BCRP (V12M, Q141K, A149P, R163K, Q166E, P269S, and S441N BCRP). Although Q141K BCRP exhibited a lower activity than wild type BCRP, no significant transport was observed for S441N BCRP (Fig. 5a). Figure 5b shows the intrinsic transport activities normalized by the expression levels of BCRP protein. There was no significant difference between wild type BCRP and SNPs variants.

DISCUSSION

In the current study, we analyzed the function of BCRP SNPs in terms of their localization, expression level, and

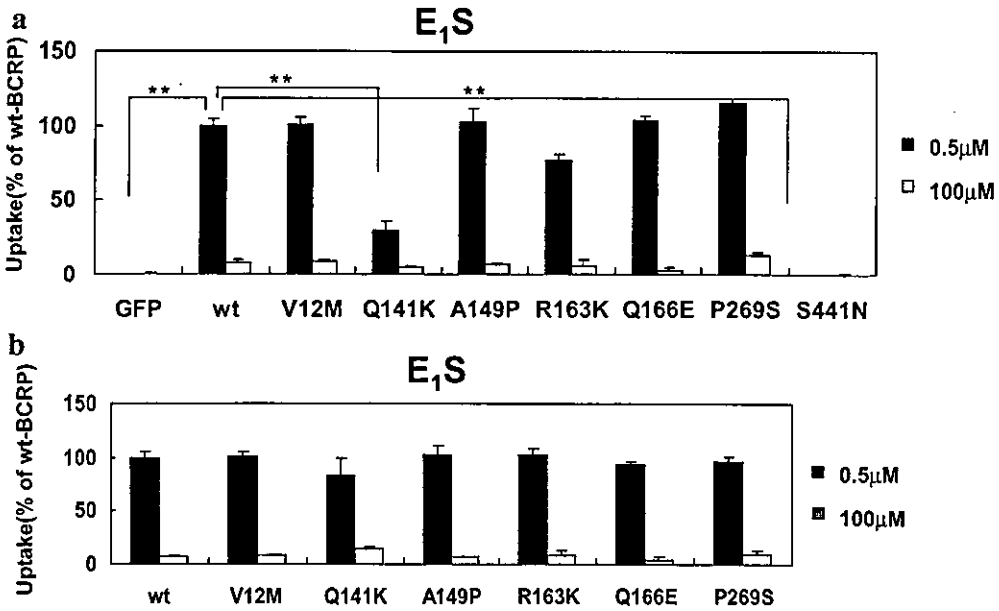

Fig. 3. The transport of E_1S by BCRP variants. The uptake of [^{3}H]E_1S by 2 μg membrane vesicles prepared from BCRP cDNA-infected and GFP cDNA-infected HEK 293 cells was examined for 2 min at 37°C in a medium containing 33 nM [^{3}H]labeled E_1S, tracer (0.5 μM) and excess concentrations (100 μM) of unlabeled E_1S. Panel 3a shows the ATP-dependent uptake of [^{3}H]E_1S by BCRP variants after normalization by the membrane protein level. The uptake was calculated by subtracting the ligand uptake in the absence of ATP from that in its presence. Panel 3b shows the ATP-dependent uptake of [^{3}H]E_1S by BCRP variants after normalization by the BCRP protein levels. For the preparation of Panel 3b, the data in Panel 3a were corrected by taking into account the BCRP protein expression level in each membrane vesicle preparation determined by the Western blot analysis (Fig. 2). Results are given as % of the wild-type BCRP. **Significantly different from wild type BCRP-expressing membrane vesicles by ANOVA followed by Dunnett's test ($p < 0.01$).

transport activity. BCRP expression systems were constructed using recombinant adenoviruses with the expectation of the high expression of the exogenous genes. Compared with the membrane vesicles isolated form the P-388 cells which were infected with BCRP cDNA by the recombinant retroviruses (11), the uptake of E_1S per mg membrane protein determined in the present study was much higher. This expression system may be useful for the analysis of functional changes in SNP variants of BCRP in a sensitive manner.

Our findings suggest that two SNP variants of BCRP may affect the function of BCRP. Q141K BCRP showed a lower expression level, which is approximately 30–40% of that of the wild type. This result is consistent with the previous report that the transfection of Q141K BCRP cDNA to PA317 cells and KB-3-1 human cells also resulted in lower expression levels (19). Recently, investigation of the expression level of BCRP in 99 Japanese placenta samples revealed that people who were homozygous for this mutation showed significantly lower expression levels of BCRP (D. Kobayashi, I. Ieiri, H. Takane, M. Kimura, Y. Norikawa, H. Tohyama, S. Irie, A. Urae, H. Suzuki, H. Kusuhara, N. Terakawa, K. Mine, K. Ohtsubo and Y. Sugiyama, data presented at 18th Annual Meeting of The Japanese Society for the Study of Xenobiotics, Sapporo, October 8–10, 2003). The clinical relevance of this *in vitro* study has major implications from the point of view of the utility of the *in vitro* system for the prediction of individual pharmacokinetic difference.

Although more detailed analysis is required to clarify the mechanism governing the reduced protein expression of Q141K BCRP, immunohistochemical staining revealed that this variant is expressed on the plasma membrane and, therefore, the altered cellular localization may not be related to the reduced protein level. It has been reported that the mRNA level of this variant is similar to that of the wild type in the transfected cells where the reduced protein level was observed (19). In addition, in the human intestine, the expression of BCRP mRNA was similar in subjects with wild type and Q141K BCRP genes, whereas there was no significant correlation between the protein and mRNA levels for BCRP (20). It has also been suggested that linkage disequilibrium is present between a CTCA deletion in the 5′-flanking region (g-19572-19569) and Q141K in Swedish subjects (21). More detailed analysis is required to clarify the mechanism for the reduced protein expression of this BCRP variant and its physiologic significance.

As far as the cellular localization was concerned, S441N BCRP was the only variant which was expressed in the intracellular compartment. We also found that the intracellular localization of S441N BCRP in HEK293 cells after transient expression (data not shown), whereas the wild-type BCRP was expressed on the cell membrane. It is possible that this variant is retained in the endoplasmic reticulum and most of the protein is degraded in the proteosomes as reported for many kinds of membrane proteins (22). Western blot analysis revealed that the expression of S441N is significantly lower than the wild type BCRP. Its expression level was reduced not only in the isolated membrane fraction, but also in the whole cell lysate (Fig. 2). These results suggest that this SNPs may

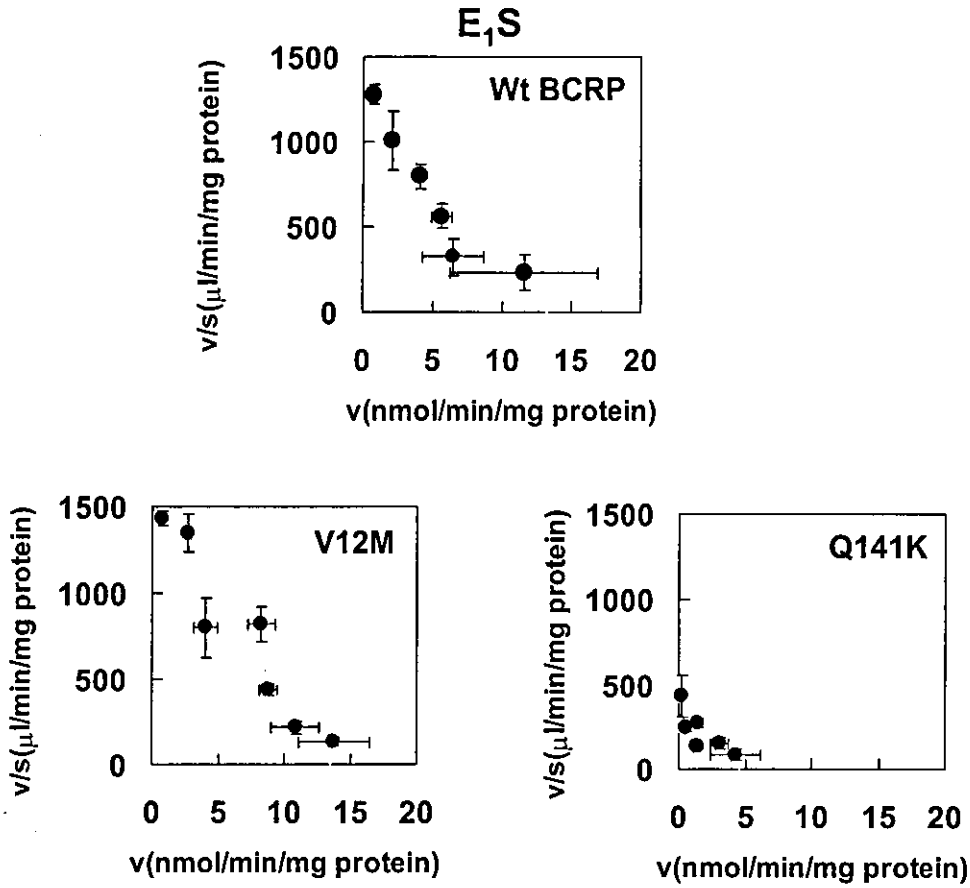

Fig. 4. Saturation of BCRP mediated transport of E_1S. Saturation of [^{3}H]E_1S transport was determined for the wild-type, V12M, and Q141K BCRP. The uptake of [^{3}H]E_1S by 2 μg membrane vesicles prepared from BCRP cDNA-infected HEK 293 cells was examined for 1 min at 37°C in a medium containing 33 nM [^{3}H]labeled E_1S and several concentrations of unlabeled E_1S. The results are given as the Eadie-Hofstee plots. Each point and bar represents the mean ± SE value of triplicate determinations.

affect both cellular localization and expression level. Concerning the cellular localization of SNPs variants of BCrP, Mizuarai *et al.* reported the intracellular localization of V12M BCRP in stably transfected LLC-PK1 cells very recently (23). The finding by Mizuarai *et al.* (23) was in marked contrast to the present finding that V12M BCRP is expressed on the apical membrane of transiently transfected LLC-PK1 cells (Fig. 1). At the present moment, we do not have any good answer to account for the discrepancy. It is possible that the cellular localization of V12M BCRP is affected by the culture conditions of LLC-PK1 cells.

Although it has been reported that the amino acid replacement at the protein of 482 alters the substrate specificity of BCRP (12,13), there has been no report on alterations in the substrate specificity due to SNP variations. In the present study, we examined the transport activity of some organic anions using isolated membrane vesicles expressing the wild type and SNP variants of BCRP. In addition to the previously described substrates such as E_1S, DHEAS and methotrexate (11), we found that PAH is also transported by BCRP. For these compounds, our results indicated that the transport activity per BCRP molecule for 6 kinds of SNP variants (V12M, A149P, R163K, Q166E, P269S, and also Q141K BCRP) is almost the same as that of the wild type BCRP (Figs. 3 and 5). In addition, the extent of the inhibition of the transport of [^{3}H]DHEAS, [^{3}H]methotrexate and [^{3}H]PAH by 80 μM DHEAS, 450 μM methtrexate and 3 mM PAH, respectively (Fig. 5), is accounted for by considering the transport char-

Fig. 5. The transport of DHEAS, MTX, and PAH by BCRP variants. The uptake of each compounds by 10 μg membrane vesicles prepared from BCRP and GFP expressing-HEK 293 cells was examined for 2 min at 37°C in a medium containing 33 nM [^{3}H]labeled compounds, tracer (0.5 μM), and excess concentrations (80 μM, 450 μM, and 3 mM, for DHEAS, MTX, and PAH, respectively) of unlabeled compounds. Panel 5a shows the ATP-dependent uptake of [^{3}H]compounds by BCRP variants after normalization by the membrane protein level. The uptake was calculated by subtracting the ligand uptake in the absence of ATP from that in its presence. Panel 5b shows the ATP-dependent uptake of these compounds by BCRP variants after normalization by the BCRP protein levels. For the preparation of Panel 5b, the uptake data were corrected by taking into account the BCRP protein expression level in each membrane vesicle preparation determined by the Western blot analysis (Fig. 2). Results are given as % of the wild type BCRP. **Significantly different from the wild type BCRP-expressing membrane vesicles by ANOVA followed by Dunnett's test ($p < 0.01$).

a

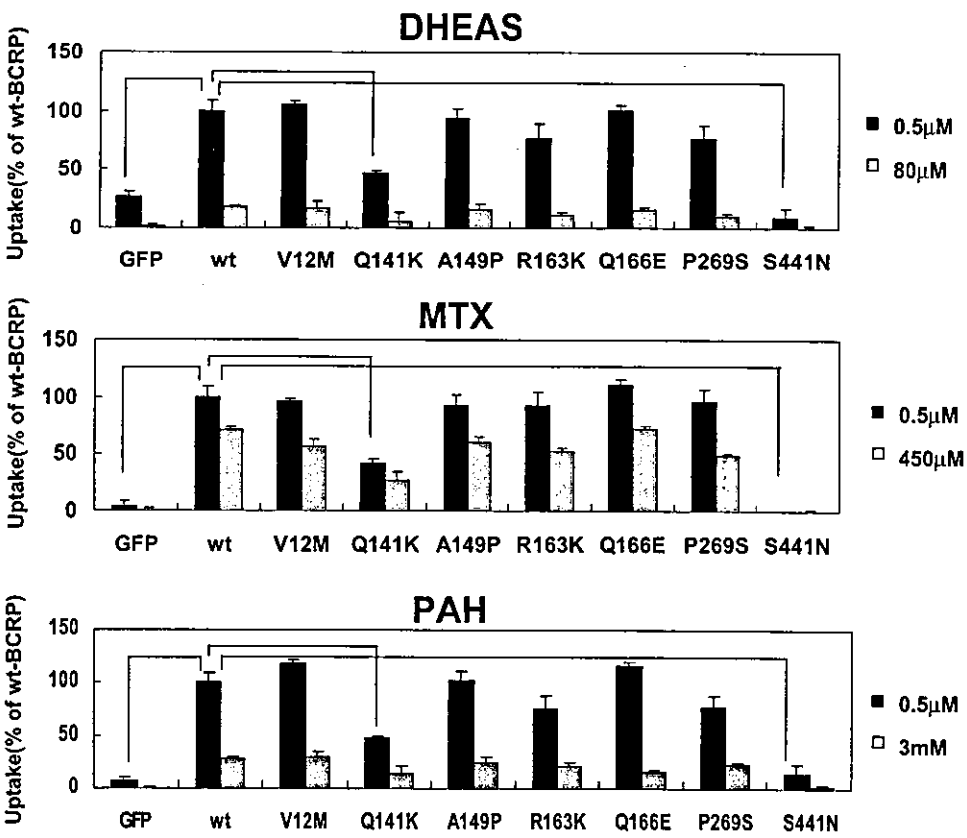
DHEAS
Uptake(% of wt-BCRP)
150
100
50
0
GFP wt V12M Q141K A149P R163K Q166E P269S S441N
0.5μM
80μM
MTX
Uptake(% of wt-BCRP)
150
100
50
0
GFP wt V12M Q141K A149P R163K Q166E P269S S441N
0.5μM
450μM
PAH
Uptake(% of wt-BCRP)
150
100
50
0
GFP wt V12M Q141K A149P R163K Q166E P269S S441N
0.5μM
3mM

b

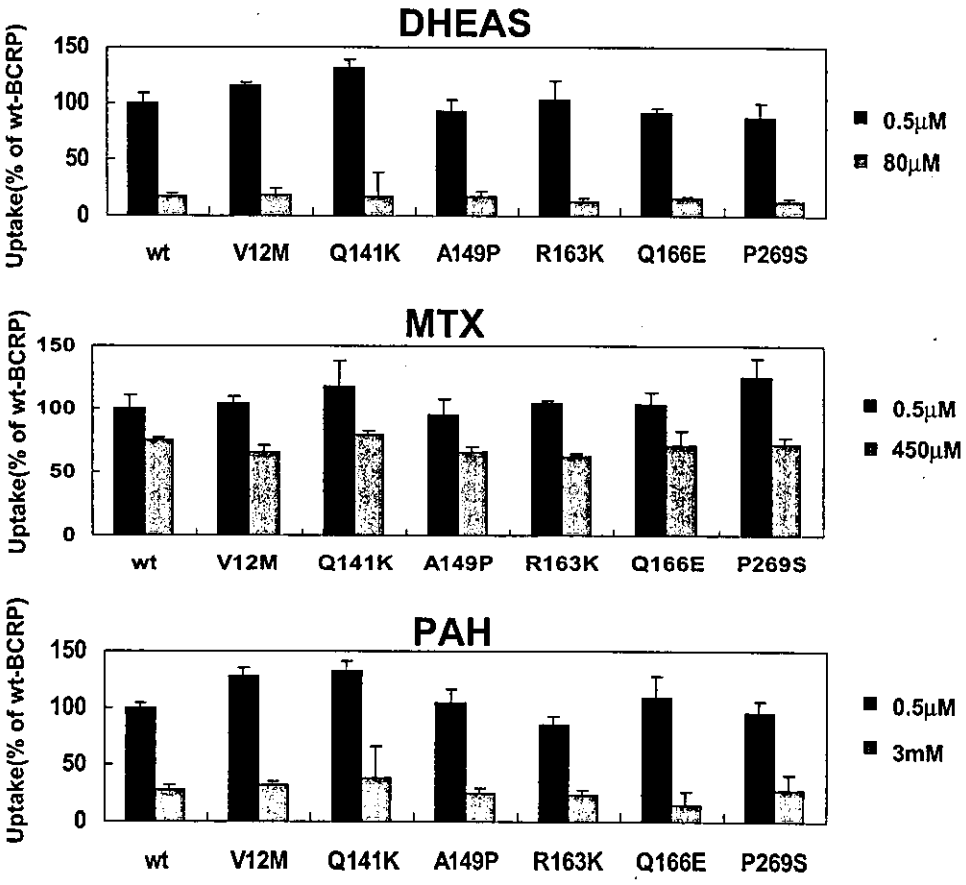
DHEAS
Uptake(% of wt-BCRP)
150
100
50
0
wt V12M Q141K A149P R163K Q166E P269S
0.5μM
80μM
MTX
Uptake(% of wt-BCRP)
150
100
50
0
wt V12M Q141K A149P R163K Q166E P269S
0.5μM
450μM
PAH
Uptake(% of wt-BCRP)
150
100
50
0
wt V12M Q141K A149P R163K Q166E P269S
0.5μM
3mM

acteristics of these compounds; we reported that DHEAS reduced the BCRP-mediated transport of [^{3}H]E_1S with an approximate IC_{50} value of 55 μM (11). The K_m value for BCRP-mediated transport of methotrexate is reported to be 0.68 ~1.34 mM (24,25). We also found that PAH is transported by BCRP with the K_m value of 3~5 mM (unpublished observations). Furthermore, the K_m values for E_1S were similar between the wild type, V12M and Q141K BCRP (Fig. 4).

It has been reported that there is a marked ethnic difference in the frequency of Q141K SNPs, and this is the prevalent allele in the Japanese population (19,21). In the present study, we constructed SNP variants of BCRP based on the information from 100 Japanese placenta specimens, 84 established cancer cell lines, and 60 Japanese individuals who received the administration of irinotecan. In particular, the frequency of the Q141K variant was 29–36% in the Japanese, whereas the frequency in 26 Caucasians subjects was only 8%. Among the 100 Japanese specimens, S441N SNPs were only found in one heterozygous subject and, consequently, their allele frequency was calculated to be only 0.5%. It is possible that the disposition of BCRP substrates is different between the subjects with the wild type BCRP and those with the SNPs variants of BCRP. One of the most important substrates for BCRP is pheophorbide a, a dietary catabolite of chlorophyll. It has been shown that the plasma concentration of pheophorbide a is increased in the Bcrp1 (–/–) mice, resulting in the occurrence of severe phototoxic ear lesions (10). Since pheophorbide a is also transported by human BCRP (10), it is likely that Q141K and S441N SNPs may be involved in the phototoxicity and protoporphyria induced by the intake of chlorophyll.

Concerning the disposition of antitumor drugs, it has also been reported that Bcrp1 (–/–) hematopoietic stem cells are sensitive to mitoxantrone-induced toxicity (26). These data suggest that the ability to protect stem cells from some genotoxic xenobiotics might be lower in subjects who have Q141K and S441N SNPs in BCRP gene. It has also been suggested that the oral absorption of topotecan is restricted by the intestinal expression of BCRP (9). This suggestion is based on the findings that, after the oral administration of both topotecan and the inhibitor of Mdr1 and Bcrp1, GF120918, the bioavailability of this antitumor drug in plasma was dramatically increased, not only in normal mice but also in Mdr1 (–/–) mice (9). It has also been reported that, in human jejunal biopsies, mRNA expression of BCRP is higher than that of MDR1 mRNA (27), suggesting the importance of BCRP in drug absorption. It has also been shown that BCRP plays an important role in placenta (9). In mdr1a/1b (–/–) mice, administration of GF120918 resulted in the higher topotecan levels in fetuses and maternal plasma. Moreover, SNPs of BCRP may also be involved in the intestinal toxicity of SN-38, an active metabolite of irinotecan. Since BCRP also transports SN-38 (28), it is possible that subjects who have Q141K or S441N SNPs variants of BCRP are more sensitive to SN-38.

In conclusion, we have shown that two kinds of SNP variants of BCRP (Q141K and S441N BCRP) are associated with the reduced expression. In particular, S441N variation is associated with the altered cellular localization. Since the allele frequency of Q141K in Japanese subjects is as high as 29-36%, it is possible that the interindividual variations in *in vivo* disposition of BCRP substrates may result from the genotype of BCRP.

ACKNOWLEDGMENTS

This work was supported by a grant-in-aid from the Ministry of Education, Science, Culture and Sports for the 21st Century Center of Excellence program and by Health and Labor Sciences Research Grants from the Ministry of Health, Labor, and Welfare for the Research on Advanced Medical Technology.

REFERENCES

1. L. A. Doyle, W. Yang, L. V. Abruzzo, T. Krogmann, Y. Gao, A. K. Rishi, and D. D. Ross. A multidrug resistance transporter from human MCF-7 breast cancer cells. *Proc. Natl. Acad. Sci. USA* **95**:15665–15670 (1998).
2. K. Miyake, T. Litman, R. Robey, and S. E. Bates. Reversal of resistance by GF120918 in cell lines expressing the ABC half-transporter, MXR. *Cancer Lett.* **146**:117–126 (1999).
3. R. Allikmets, L. M. Schriml, A. Hutchinson, V. Romano-Spica, and M. Dean. A human placenta-specific ATP-binding cassette gene (ABCP) on chromosome 4q22 that is involved in multidrug resistance. *Cancer Res.* **58**:5337–5339 (1998).
4. J. D. Allen, R. F. Brinkhuis, J. Wijnholds, and A. H. Schinkel. The mouse Bcrp1/Mxr/Abcp gene: amplification and overexpression in cell lines selected for resistance to topotecan, mitoxantrone, or doxorubicin. *Cancer Res.* **59**:4237–4241 (1999).
5. K. J. Bailey-Dell, B. Hassel, L. A. Doyle, and D. D. Ross. Promoter characterization and genomic organization of the human breast cancer resistance protein (ATP-binding cassette transporter G2) gene. *Biochim. Biophys. Acta* **1520**:234–241 (2001).
6. K. Kage, S. Tsukahara, T. Sugiyama, S. Asada, E. Ishikawa, T. Tsuruo, and Y. Sugimoto. Dominant-negative inhibition of breast cancer resistance protein as drug efflux pump through the inhibition of S-S dependent homodimerization. *Int. J. Cancer* **97**:626–630 (2002).
7. T. Litman, T. E. Druley, W. D. Stein, and S. E. Bates. From MDR to MXR: new understanding of multidrug resistance systems, their properties and clinical significance. *Cell. Mol. Life Sci.* **58**: 931–959 (2001).
8. M. Maliepaard, G. L. Scheffer, I. F. Faneyte, M. A. van Gastelen, A. C. Pijnenborg, A. H. Schinkel, M. J. van De Vijver, R. J. Scheper, and J. H. Schellens. Subcellular localization and distribution of the breast cancer resistance protein transporter in normal human tissues. *Cancer Res.* **61**:3458–3464 (2001).
9. J. W. Jonker, J. W. Smit, R. F. Brinkhuis, M. Maliepaard, J. H. Beijnen, J. H. Schellens, and A. H. Schinkel. Role of breast cancer resistance protein in the bioavailability and fetal penetration of topotecan. *J. Natl. Cancer Inst.* **92**:1651–1656 (2000).
10. J. W. Jonker, M. Buitelaar, E. Wagenaar, M. A. van der Valk, G. L. Scheffer, R. J. Scheper, T. Plosch, F. Kuipers, R. P. Oude Elferink, H. Rosing, J. H. Beijnen, and A. H. Schinkel. The breast cancer resistance protein protects against a major chlorophyll-derived dietary phototoxin and protoporphyria. *Proc. Natl. Acad. Sci. USA* **99**:15649–15654 (2002).
11. M. Suzuki, H. Suzuki, Y. Sugimoto, and Y. Sugiyama. ABCG2 transports sulfated conjugates of steroids and xenobiotics. *J. Biol. Chem.* **278**:22644–22649 (2003).
12. Y. Honjo, C. A. Hrycyna, Q. W. Yan, W. Y. Medina-Perez, R. W. Robey, A. van de Laar, T. Litman, M. Dean, and S. E. Bates. Acquired mutations in the MXR/BCRP/ABCP gene alter substrate specificity in MXR/BCRP/ABCP-overexpressing cells. *Cancer Res.* **61**:6635–6639 (2001).
13. H. Mitomo, R. Kato, A. Ito, S. Kasamatsu, Y. Ikegami, I. Kii, A. Kudo, E. Kobatake, Y. Sumino, and T. Ishikawa. A functional study on polymorphism of the ATP-binding cassette transporter ABCG2: critical role of arginine-482 in methotrexate transport. *Biochem. J.* **373**:767–774 (2003).
14. M. Itoda, Y. Saito, K. Shirao, H. Minami, A. Ohtsu, T. Yoshida, N. Saijo, H. Suzuki, Y. Sugiyama, S. Ozawa, and J.-I. Sawada. Eight novel single nucleotide polymorphisms in *ABCG2/BCRP* in Japanese cancer patients administered irinotecan. *Drug Metab. Pharmacokinet.* **18**:212–217 (2003).
15. H. Mizuguchi and M. A. Kay. Efficient construction of a recom-

binant adenovirus vector by an improved in vitro ligation method. *Hum. Gene Ther.* **9**:2577–2583 (1998).
16. H. Mizuguchi and M. A. Kay. A simple method for constructing E1- and E1/E4-deleted recombinant adenoviral vectors. *Hum. Gene Ther.* **10**:2013–2017 (1999).
17. M. Muller, C. Meijer, G. J. Zaman, P. Borst, R. J. Scheper, N. H. Mulder, E. G. de Vries, and P. L. Jansen. Overexpression of the gene encoding the multidrug resistance-associated protein results in increased ATP-dependent glutathione S-conjugate transport. *Proc. Natl. Acad. Sci. USA* **91**:13033–13037 (1994).
18. T. Hirohashi, H. Suzuki, X. Y. Chu, I. Tamai, A. Tsuji, and Y. Sugiyama. Function and expression of multidrug resistance-associated protein family in human colon adenocarcinoma cells (Caco-2). *J. Pharmacol. Exp. Ther.* **292**:265–270 (2000).
19. Y. Imai, M. Nakane, K. Kage, S. Tsukahara, E. Ishikawa, T. Tsuruo, Y. Miki, and Y. Sugimoto. C421A polymorphism in the human breast cancer resistance protein gene is associated with low expression of Q141K protein and low-level drug resistance. *Mol. Cancer Ther.* **1**:611–616 (2002).
20. C. P. Zamber, J. K. Lamba, K. Yasuda, J. Farnum, K. Thummel, J. D. Schuetz, and E. G. Schuetz. Natural allelic variants of breast cancer resistance protein (BCRP) and their relationship to BCRP expression in human intestine. *Pharmacogenetics* **13**:19–28 (2003).
21. G. Backstrom, J. Taipalensuu, H. Melhus, H. Brandstrom, A. C. Svensson, P. Artursson, and A. Kindmark. Genetic variation in the ATP-binding Cassette Transporter gene ABCG2 (BCRP) in a Swedish population. *Eur. J. Pharm. Sci.* **18**:359–364 (2003).
22. K. Hashimoto, T. Uchiumi, T. Konno, T. Ebihara, T. Nakamura, M. Wada, S. Sakisaka, F. Maniwa, T. Amachi, K. Ueda, and M. Kuwano. Trafficking and functional defects by mutations of the ATP-binding domains in MRP2 in patients with Dubin-Johnson syndrome. *Hepatology* **36**:1236–1245 (2002).
23. S. Mizuarai, N. Aozasa, and H. Kotani. Single nucleotide polymorphisms result in impaired membrane localization and reduced ATPase activity in multidrug transporter ABCG2. *Int. J. Cancer* **109**:238–246 (2004).
24. E. L. Volk and E. Schneider. Wild-type breast cancer resistance protein (BCRP/ABCG2) is a methorexate polyglutamate transporter. *Cancer Res.* **63**:5538–5543 (2003).
25. Z. S. Chen, R. W. Robey, M. G. Belinsky, I. Shchaveleva, X. Q. Ren, Y. Sugimoto, D. D. Ross, S. E. Bates, and G. D. Kruh. Transport of methotrexate, methotrexate polyglutamates, and 17β estraciol 17β-D-glucuronide by ABCG2: effects of acquired mutations at R482 on methotrexate transport. *Cancer Res.* **64**: 4048–4054 (2003).
26. S. Zhou, J. J. Morris, Y. Barnes, L. Lan, J. D. Schuetz, and B. P. Sorrentino. Bcrp1 gene expression is required for normal numbers of side population stem cells in mice, and confers relative protection to mitoxantrone in hematopoietic cells in vivo. *Proc. Natl. Acad. Sci. USA* **99**:12339–12344 (2002).
27. J. Taipalensuu, H. Tornblom, G. Lindberg, C. Einarsson, F. Sjoqvist, H. Melhus, P. Garberg, B. Sjostrom, B. Lundgren, and P. Artursson. Correlation of gene expression of ten drug efflux proteins of the ATP-binding cassette transporter family in normal human jejunum and in human intestinal epithelial Caco-2 cell monolayers. *J. Pharmacol. Exp. Ther.* **299**:164–170 (2001).
28. K. Nakatomi, M. Yoshikawa, M. Oka, Y. Ikegami, S. Hayasaka, K. Sano, K. Shiozawa, S. Kawabata, H. Soda, T. Ishikawa, S. Tanabe, and S. Kohno. Transport of 7-ethyl-10-hydroxycamptothecin (SN-38) by breast cancer resistance protein ABCG2 in human lung cancer cells. *Biochem. Biophys. Res. Commun.* **288**:827–832 (2001).

0022-3565/04/3111-228–236$20.00
THE JOURNAL OF PHARMACOLOGY AND EXPERIMENTAL THERAPEUTICS
Vol. 311, No. 1
68536/1171497
Printed in U.S.A.

JPET 311:228–236, 2004

Gemfibrozil and Its Glucuronide Inhibit the Organic Anion Transporting Polypeptide 2 (OATP2/OATP1B1:*SLC21A6*)-Mediated Hepatic Uptake and CYP2C8-Mediated Metabolism of Cerivastatin: Analysis of the Mechanism of the Clinically Relevant Drug-Drug Interaction between Cerivastatin and Gemfibrozil

Yoshihisa Shitara, Masaru Hirano, Hitoshi Sato, and Yuichi Sugiyama

School of Pharmaceutical Sciences, Showa University, Tokyo, Japan (Y.Sh., H.S.); and Graduate School of Pharmaceutical Sciences, The University of Tokyo, Tokyo, Japan (M.H., Y.Su.)

Received March 16, 2004; accepted June 10, 2004

ABSTRACT

A serious pharmacokinetic interaction between cerivastatin (CER) and gemfibrozil (GEM) has been reported. In the present study, we examined the inhibitory effects of GEM and its metabolites, M3 and gemfibrozil 1-*O*-β-glucuronide (GEM-1-*O*-glu), on the uptake of CER by human organic anion transporting polypeptide 2 (OATP2)-expressing cells and its metabolism in cytochrome P450 expression systems. Uptake studies showed that GEM and GEM-1-O-glu significantly inhibited the OATP2-mediated uptake of CER with IC_{50} values of 72 and 24 μM, respectively. They also inhibited the CYP2C8-mediated metabolism of CER with IC_{50} values of 28 and 4 μM, respectively, whereas M3 had no effects. GEM and GEM-1-*O*-glu minimally inhibited the CYP3A4-mediated metabolism of CER. The IC_{50} values of GEM and GEM-1-*O*-glu for the uptake and the metabolism of CER obtained in the present study were lower than their total, and not unbound, plasma concentrations. However, considering the possibly concentrated high unbound concentrations of GEM-1-*O*-glu in the liver and its relatively larger plasma unbound fraction compared with GEM itself, the glucuronide inhibition of the CYP2C8-mediated metabolism of CER appears to be the main mechanism for the clinically relevant drug-drug interaction. Previously reported clinical drug interaction studies showing that coadministration of GEM with pravastatin or pitavastatin, both of which are known to be cleared from the plasma by the uptake transporters in the liver, only minimally (less than 2-fold) increased the area under the plasma concentration-time curve of these statins, also supported our present conclusion.

3-Hydroxy-3-methylglutaryl CoA reductase inhibitors (statins) and fibrates are now well established treatments for hyperlipidemia to prevent cardiovascular diseases (Wierzbicki et al., 2003). Statins are principally used to reduce low density lipoprotein and also triglycerides in proportion to their low density lipoprotein-lowering efficacy and the baseline triglyceride level, whereas fibrates are mainly used for the treatment of hypertriglyceridemia or as second-line agents in patients with statin intolerance (Moghadasian et al., 2000; Wierzbicki et al., 2003). The combination therapy of statins and fibrates is widely used in clinical practice; however, there are reports of rhabdomyolysis by this combination therapy, mainly involving gemfibrozil (GEM) with lovastatin and cerivastatin (CER) (Abdul-Ghaffar and El-Sonbaty, 1995; Bruno-Joyce et al., 2001; Roca et al., 2002). This may be partly due to drug-drug interactions (DDI) caused by events at a pharmacokinetic level, although an event at a pharmacodynamic

This study was supported in part by a grant-in-aid for Young Scientists (B) provided by the Ministry of Education, Culture, Sports, Science and Technology, Japan (Y.Sh.), a grant-in-aid for the Advanced and Innovational Research Program in Life Sciences from the Ministry of Education, Culture, Sports, Science and Technology, Japan (Y.Su.), and a Health and Labor Sciences Research grant from the Ministry of Health, Labor and Welfare, Japan, for the Research on Advanced Medical Technology (Y.Su.).

Article, publication date, and citation information can be found at http://jpet.aspetjournals.org.

doi:10.1124/jpet.104.068536.

ABBREVIATIONS: GEM, gemfibrozil; CER, cerivastatin; DDI, drug-drug interaction; AUC, area under the plasma concentration-time curve; P450, cytochrome P450; UGT, uridine diphosphate glucuronosyltransferase; K_i, inhibition constant; GEM-1-*O*-glu, gemfibrozil 1-*O*-β-glucuronide; HPLC, high-performance liquid chromatography; IC_{50}, concentration of inhibitor to produce a 50% reduction in the metabolism or transport; HLM, human liver microsome; Ab, antibody; TLC, thin-layer chromatography; CL_{uptake}, uptake clearance.

level, i.e., a strong direct effect on myocytes by combination therapy, may be also involved (Kyrklund et al., 2001; Backman et al., 2002; Matzno et al., 2003). Indeed, concomitant use of GEM markedly increased the area under the plasma concentration-time curve (AUC) of simvastatin acid, lovastatin acid, and CER and produced a small increase in the concentrations of pravastatin and pitavastatin (Backman et al., 2000, 2002; Kyrklund et al., 2001, 2003; Mathew et al., 2004). Staffa et al. (2002) reported that 31 patients taking CER died due to rhabdomyolysis, and 12 of them were concomitantly taking GEM. Due to this severe side effect, CER was voluntarily withdrawn from the world market in August 2001.

Reports have appeared describing the mechanism of the pharmacokinetic interaction between CER and GEM (Wen et al., 2001; Prueksaritanont et al., 2002b,c; Wang et al., 2002). In humans, CER is subject to a dual metabolic pathway mediated by CYP2C8 and CYP3A4 (Mück, 2000). Wen et al. (2001) and Wang et al. (2002) reported that GEM inhibits multiple isoforms of cytochromes P450 (P450s), including CYP2C8, but has no inhibitory effect on CYP3A4. Therefore, the inhibition of CYP2C8-mediated metabolism may be one mechanism responsible for this clinically relevant DDI. In addition, Prueksaritanont et al. (2002a) have suggested that UGT-mediated glucuronidation of statins is an important metabolic pathway because they are spontaneously converted to lactones following UGT-mediated glucuronidation. Prueksaritanont et al. (2002b,c) have also reported that GEM inhibits this UGT-mediated glucuronidation of CER as well as P450-mediated oxidation. The inhibition constants (K_i) or the concentrations of inhibitors to produce a 50% reduction in the metabolism of CER (IC_{50}) in their reports were as high as the total plasma concentration of GEM in the therapeutic range (Prueksaritanont et al., 2002b,c; Wang et al., 2002); however, taking the high protein binding of GEM into consideration, the unbound concentration of GEM is much less than the reported K_i or IC_{50} values (Todd and Ward, 1988; Prueksaritanont et al., 2002c; Wang et al., 2002).

We previously reported that CER was actively taken up into the liver via transporter(s) including organic anion transporting polypeptide 2 [OATP2 (OATP1B1); *SLC21A6*] (Shitara et al., 2003). We investigated the inhibitory effects of cyclosporin A on the transporter-mediated uptake of CER in hepatocytes and showed that cyclosporin A inhibited it without any effects on its metabolism at therapeutic concentrations (Shitara et al., 2003). This partly explained the mechanism responsible for the clinically relevant DDI between CER and cyclosporin A (Shitara et al., 2003); however, there have been no reports of the interaction between GEM and transporters until now. Gemfibrozil 1-*O*-β-glucuronide (GEM-1-*O*-glu), a metabolite of GEM, is taken up and accumulates in isolated perfused rat liver (Sallustio et al., 1996; Sabordo et al., 1999, 2000). This uptake is inhibited by coadministration of dibromosulfophthalein and clofibric acid, whereas acetaminophen and its glucuronide produced no inhibition (Sabordo et al., 1999, 2000). These results suggest an involvement of transporter(s) in the hepatic uptake of GEM-1-*O*-glu, and therefore, GEM-1-*O*-glu may affect the transporter-mediated uptake of CER.

GEM is metabolized to M1–4 by P450s with M3 being the major metabolite (Nakagawa et al., 1991). GEM also undergoes glucuronidation, mainly to GEM-1-*O*-glu (Nakagawa et al., 1991), and the plasma concentrations of these metabolites are reported to be relatively high (Okerholm et al., 1976; Nakagawa et al., 1991). Therefore, in the present study, we examined the effects of GEM and its major metabolites, M3 and GEM-1-*O*-glu, on the metabolism and the transporter-mediated uptake of CER to analyze the mechanism of the clinically relevant DDI between CER and GEM.

Materials and Methods

Materials. [^{14}C]CER (2.03 GBq/mmol) and unlabeled CER were kindly provided by Bayer AG (Wuppertal, Germany). GEM was purchased from Sigma-Aldrich (St. Louis, MO). A metabolite of GEM, M3 (purity: 99.6%), was chemically synthesized in KNC Laboratories, Co. Ltd. (Kobe, Japan). GEM-1-*O*-glu was enzymatically synthesized from GEM. GEM (2 mg/ml) was incubated at 37°C with rat microsomes (3.6 mg of protein/ml) and 5 mg/ml UDP glucuronic acid in 100 mM glycine-NaOH buffer (pH 8.5) supplemented with 20% (w/v) glycerin for 27 h, followed by the addition of 1 N HCl to bring the pH to 4.0. This sample was chromatographed on an ODS column (Cosmosil 75C_{18}-PREP, 300 ml; Nakalai Tesque, Kyoto, Japan) with MeOH/H_2O (30:70–80:20, stepwise) as the mobile phase and analyzed by high-performance liquid chromatography (HPLC) using an ODS column (Inertsil ODS-2, ϕ4.6 × 150 mm; GL Sciences, Inc., Tokyo, Japan) with a mobile phase of 0.05% trifluoroacetic acid/acetonitrile (53:47) at a flow rate of 1.0 ml/min. The fraction containing GEM-1-*O*-glu, detected by its absorbance at 254 nm, was collected and evaporated. The fraction was rechromatographed on an ODS column with MeOH/H_2O (50:50–80:20, stepwise) and purified, followed by evaporation, to obtain GEM-1-*O*-glu. The purity was 99.4% determined by HPLC detected by the absorbance at 230 nm. The chemical structures and molecular weights of M3 and GEM-1-*O*-glu were confirmed by NMR and mass spectrometry (MS) analyses, respectively. The chemical structures of GEM and its metabolites used in the present study are shown in Fig. 1. All other reagents were of analytical grade.

Uptake of [^{14}C]CER in OATP2-Expressing Cells. An uptake study of CER in OATP2-expressing cells was conducted in the presence of GEM and its metabolites, M3 and GEM-1-*O*-glu. The construction of OATP2-expressing Madin-Darby canine kidney (MDCK) cells has been previously described (Sasaki et al., 2002). The uptake of [^{14}C]CER was examined by the method described previously (Shitara et al., 2003). The inhibitors, GEM (0–300 μM), M3 (0–1000 μM), or GEM-1-*O*-glu (0–300 μM), were added along with [^{14}C]CER when the uptake reaction was initiated.

In Vitro Metabolism of CER. To measure the effect of GEM and its metabolites on the metabolism of [^{14}C]CER and to estimate the contributions of CYP2C8 and 3A4, its in vitro metabolism was examined in CYP2C8- and 3A4-expressing insect cells supplemented with the expression of human P450 reductase and cytochrome b_5 (Supersome; BD Gentest, Woburn, MA) and pooled human liver microsomes (HLM; BD Gentest). To estimate the contribution of CYP2C8, HLM was preincubated with a specific inhibitory antibody (Ab) against CYP2C8 (BD Gentest; 0–10 μl/0.1 mg protein HLM) at 4°C for 20 min. To estimate the contribution of CYP3A4, ketoconazole (0–1 μM), a potent CYP3A4 inhibitor, was used. Prior to the metabolism study, human CYP2C8 and 3A4 expression systems (final 20 nM P450) or HLM (final 0.2 mg of protein/ml) were incubated at 37°C for 10 min in 100 mM potassium phosphate buffer (pH 7.4) containing 3.3 mM $MgCl_2$, 3.3 mM glucose 6-phosphate, 0.4 U/ml glucose-6-phosphate dehydrogenase, 1.3 mM NADPH, and 0.8 mM NADH. A 500-μl volume of incubation mixture was transferred to a polyethylene tube, and [^{14}C]CER (0.25 μM) was added to initiate the reaction with GEM, M3, or GEM-1-*O*-glu (0–300 μM). After incubation for 30 min, the reaction was terminated by the addition of 500 μl of ice-cold acetonitrile because this method had been shown to terminate the enzymatic reaction in a pilot study (data not shown),

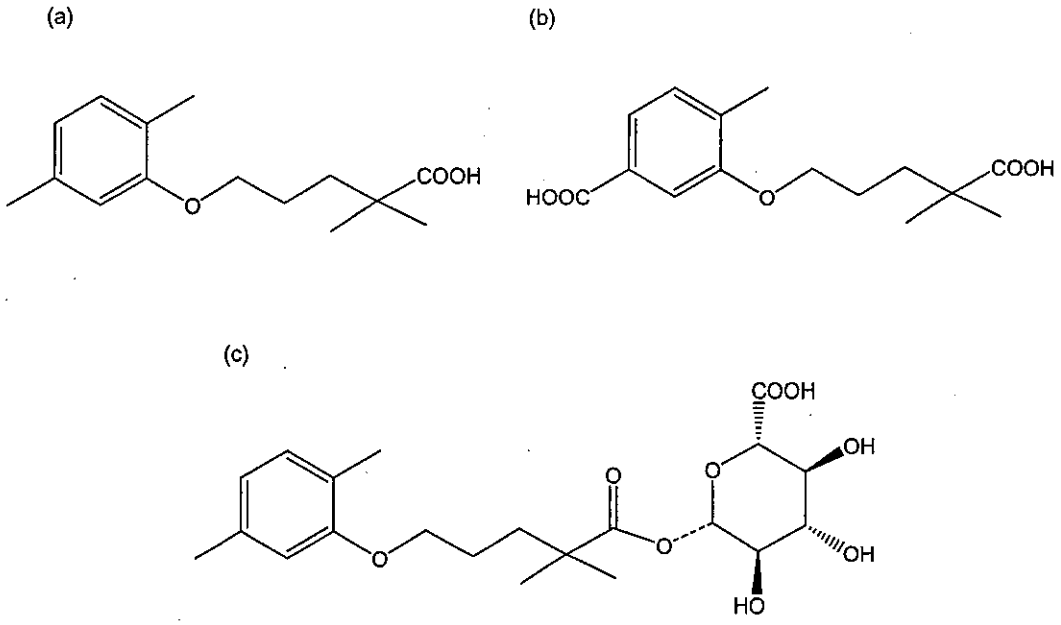

Fig. 1. Chemical structures of GEM and its metabolites. a, GEM; b, M3; c, GEM-1-*O*-glu.

subsequently followed by centrifugation. To measure the metabolic rate of [^{14}C]CER, the supernatant was collected and concentrated to approximately 20 μl in a centrifugal concentrator (VC-36N; TAITEC, Saitama, Japan), followed by thin-layer chromatography (TLC). The analyte was separated on silica gel 60F_{254} (Merck KGaA, Darmstadt, Germany) using a suitable mobile phase (toluene/acetone/acetic acid, 70:30:5, v/v). The intensity of the bands for intact [^{14}C]CER and its metabolites separated by TLC was determined by the BAS 2000 system (Fuji Film, Tokyo, Japan).

Protein Binding of GEM and Its Metabolites. To estimate the fraction not bound to human serum protein, 300 μM GEM, M3, and GEM-1-*O*-glu were added to serum (Nissui Pharmaceuticals, Inc., Tokyo, Japan), buffered with 50 mM potassium phosphate at 37°C, and incubated for 2 min. After that, the sample underwent ultrafiltration (Amicon Centrifree; Millipore Corporation, Billerica, MA) and the GEM and its metabolites in the filtrate were determined by HPLC. Phosphate-buffered saline (0.5 ml) containing 5 μl of 1 mM ibuprofen (internal standard) and 20 μl of formic acid were added to 0.5 ml of filtrate, followed by vigorous shaking. Subsequently, the sample was extracted with 5 ml of ethyl acetate/cyclohexane (20:80); then 4 ml of the organic phase was collected and evaporated. The sample obtained was dissolved in 0.5 ml of acetonitrile and separated on an ODS column (Super ODS column, ϕ4.6 × 150 mm; Tosoh, Tokyo, Japan). The mobile phase for GEM was 10 mM acetate buffer (pH 4.7)/acetonitrile (55:45), whereas that for M3 and GEM-1-*O*-glu was a mixture of 10 mM acetate buffer (pH 4.7) and acetonitrile with a linear gradient from 70 to 55% acetate buffer for 30 min, and the flow rate was 1.0 ml/min for all analyses. The retention times for GEM and ibuprofen were 28 and 13 min, respectively, and those for M3, GEM-1-*O*-glu, and ibuprofen were 13.5, 10, and 31 min, respectively. The absorbance was measured at 254 nm, and quantitation was carried out by comparison with the absorbance of a standard curve prepared for each compound.

Data Analysis. The time courses of the uptake of [^{14}C]CER into OATP2-expressing cells were expressed as the uptake volume (μl/mg protein) of radioactivity taken up into the cells (dpm/mg protein) divided by the concentration of radioactivity in the incubation buffer (dpm/μl). The uptake velocity of [^{14}C]CER was calculated using the uptake volume obtained at 2 min and expressed as the uptake clearance (CL_{uptake}: μl/min/mg protein). The metabolic rate of [^{14}C]CER was calculated by the decrease in unchanged [^{14}C]CER or the formation of its metabolites, M1 and M23.

To calculate the IC_{50} values of GEM and its metabolites in terms of the OATP2-mediated uptake, the following equation was used:

$$\Delta CL_{uptake}(+\text{inhibitor}) = \frac{\Delta CL_{uptake}(\text{control})}{1 + I/IC_{50}} \quad (1)$$

where ΔCL_{uptake} is the CL_{uptake} for OATP2-mediated uptake, which is the CL_{uptake} of [^{14}C]CER minus that estimated in the presence of excess unlabeled CER, ΔCL_{uptake}(+inhibitor) and ΔCL_{uptake}(control) are the ΔCL_{uptake} values estimated in the presence and absence of inhibitors, respectively, and I is the inhibitor concentrations.

For the inhibitory effects of GEM and its metabolites on the metabolism of [^{14}C]CER in CYP2C8 and 3A4 expression systems, the IC_{50} values were calculated from the following equation:

$$v(+\text{inhibitor}) = \frac{v(\text{control})}{1 + I/IC_{50}} \quad (2)$$

where v(+inhibitor) and v(control) are the metabolic rates of CER in the presence and absence of inhibitors, respectively.

These equations were fitted to the data obtained in the present study using a computerized version of the nonlinear least-squares method, WinNonlin (Pharsight, Mountain View, CA) to obtain the IC_{50} values with computer-calculated S.D. values.

For the inhibition study using pooled HLM, the observed values of the metabolic rates were compared with the simulated values using the following equation:

$$v(+\text{inhibitor}) = v(\text{control}) \times \left(\frac{R_{CYP2C8}}{1 + I/IC_{50\_2C8}} + \frac{R_{CYP3A4}}{1 + I/IC_{50\_3A4}} \right) \quad (3)$$

where, R_{CYP2C8} and R_{CYP3A4} are the contributions of CYP2C8 and 3A4 to the metabolism of CER (total metabolism and the formations of M1 and M23), respectively, and IC_{50_2C8} and IC_{50_3A4} are the IC_{50} values for CYP2C8- and 3A4-mediated metabolism of CER, respectively. For this simulation, the contributions of CYP2C8 and 3A4 to the formation of M1 and M23 in HLM were calculated based on the contributions of these enzymes to the total metabolism of CER in HLM and the ratio of the initial formation rate of each metabolite in P450 expression systems to that in HLM.

Results

Inhibitory Effects of GEM and Its Metabolites on OATP2-Mediated Uptake of [^{14}C]CER. The effects of GEM, M3, and its glucuronide on the OATP2-mediated uptake of [^{14}C]CER were examined (Fig. 2). GEM and GEM-1-*O*-glu significantly inhibited OATP2-mediated uptake of [^{14}C]CER without any effects on the uptake in vector-transfected cells, whereas M3 did not show a statistically significant inhibition up to a concentration of 1000 μM (Fig. 2). The IC_{50} values of GEM and GEM-1-*O*-glu for the OATP2-mediated uptake of [^{14}C]CER were 72.4 ± 28.4 and 24.3 ± 19.8 μM, respectively (mean ± S.D.).

Inhibitory Effects of GEM and its Metabolites on the in Vitro Metabolism of [^{14}C]CER in CYP2C8 and 3A4 Expression Systems. The in vitro metabolism of [^{14}C]CER was examined in CYP2C8 and 3A4 expression systems. In the TLC analysis, one band for parent [^{14}C]CER and two other bands for metabolites were detected in the CYP2C8 expression system, whereas one band for [^{14}C]CER and only one band for a metabolite were detected in the CYP3A4 expression system. The band for one of the metabolites produced by CYP2C8 and CYP3A4 matched, suggesting that these two enzymes produced the same metabolite. This metabolite was identified as M1 and the other was M23. The Rf values for [^{14}C]CER, M1, and M23 were 0.13, 0.09, and 0.055, respectively. In Fig. 3, the metabolism of [^{14}C]CER in the CYP2C8 and 3A4 expression systems in the presence or absence of GEM and its metabolites are shown. GEM and GEM-1-*O*-glu significantly inhibited the metabolism of [^{14}C]CER in CYP2C8 and 3A4 expression systems, whereas M3 had no effects (Fig. 3). GEM and GEM-1-*O*-glu preferentially inhibited CYP2C8-mediated metabolism compared with CYP3A4-mediated metabolism (Fig. 3). The IC_{50} values of GEM and GEM-1-*O*-glu for the CYP2C8-mediated metabolism were 28.0 ± 4.3 and 4.07 ± 1.23 μM (mean ± S.D.), respectively, and the corresponding values for the CYP3A4-mediated metabolism were 372 ± 100 and 243 ± 59 μM (mean ± S.D.), respectively. In Figs. 4 and 5, the CYP2C8-mediated M1 and M23 formation rates and the CYP3A4-mediated M1 formation rate in the presence or absence of GEM and GEM-1-*O*-glu are shown. GEM and GEM-1-*O*-glu inhibited CYP2C8-mediated M1 formation with IC_{50} values of 36.8 ± 5.3 and 5.38 ± 1.29 μM (mean ± S.D.), respectively, and M23 formation with IC_{50} values of 29.7 ± 4.4 and 4.30 ± 1.48 μM (mean ± S.D.), respectively (Fig. 4). They slightly inhibited CYP3A4-mediated M1 formation with IC_{50} values of 406 ± 106 and 267 ± 62 μM (mean ± S.D.), respectively (Fig. 5). The IC_{50} values of GEM and GEM-1-*O*-glu for the OATP2-mediated uptake and the CYP2C8- and 3A4-mediated metabolism of [^{14}C]CER are summarized in Table 1.

Estimation of the Contributions of CYP2C8 and 3A4 to the Metabolism of [^{14}C]CER in Pooled HLM. To estimate the contributions of CYP2C8 and 3A4, we examined the effect of a specific inhibitory Ab for CYP2C8 and ketoconazole, a potent inhibitor of CYP3A4, on the metabolism of [^{14}C]CER in the pooled HLM (Fig. 6). Incubation with HLM produced three different metabolites detected by TLC, and one of them (Rf = 0.04) was identified as M24, a metabolite spontaneously produced from M1 and M23. In the present analysis, only the formation of M1 and M23 was analyzed. The inhibitory Ab for CYP2C8 inhibited the microsomal metabolism of [^{14}C]CER in a concentration-dependent manner at low concentrations, and maximum inhibition was obtained at 5 μl/100 μg of microsomes (Fig. 6a). At maximum inhibition, the microsomal metabolism of [^{14}C]CER decreased to 38.9 ± 2.7% (mean ± S.E.) of the control (Fig. 6a), and therefore, the contribution of CYP2C8 was estimated to be 61%. In the presence of inhibitory Ab for CYP2C8, M23 formation was completely inhibited, whereas M1 formation fell only to 61.2 ± 2.9% (mean ± S.E.) of the control (Fig. 6, b and c). Ketoconazole also reduced the microsomal metabolism of [^{14}C]CER in a concentration-dependent manner (Fig. 6d). However, the inhibition studies using CYP2C8 and 3A4 expression systems showed that it inhibited not only CYP3A4-mediated metabolism but also that mediated by CYP2C8 (Fig. 6d). At 0.1 μM, most of the CYP3A4-mediated metabolism of [^{14}C]CER was inhibited with only a minimal effect on that mediated by CYP2C8 (Fig. 6d); therefore, 0.1 μM ketoconazole was used to estimate the contribution of CYP3A4. It was found that 0.1 μM ketoconazole reduced the metabolism of [^{14}C]CER to 63.4 ± 7.2% (mean ± S.E.) of the control (Fig. 6d), suggesting that the contribution of CYP3A4

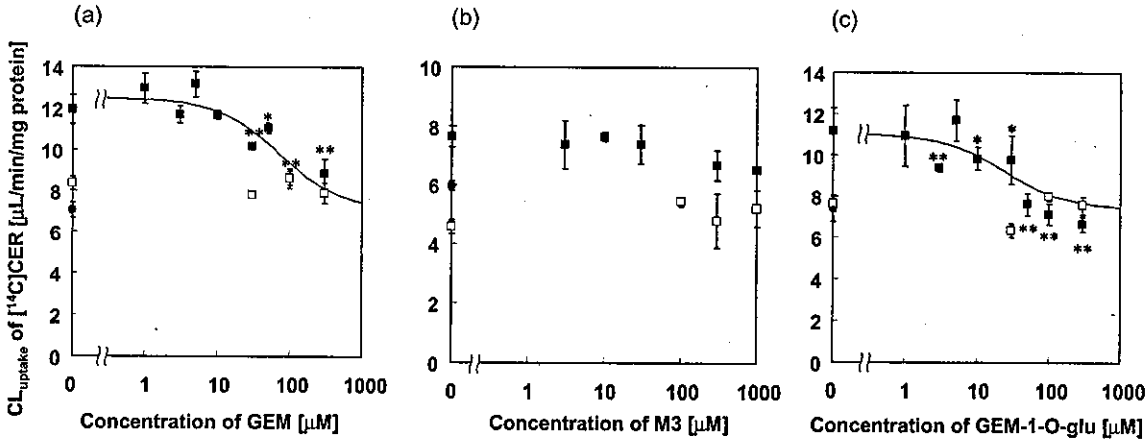

Fig. 2. Effect of GEM and its metabolites on the OATP2-mediated uptake of [^{14}C]CER. The inhibitory effects of GEM (a), M3 (b), and GEM-1-*O*-glu (c) on the OATP2-mediated uptake of [^{14}C]CER were examined. Uptake of [^{14}C]CER in OATP2-expressing (■) and vector-transfected (□) cells in the presence of GEM and its metabolites is shown. Uptake of [^{14}C]CER in the presence of excess unlabeled CER (30 μM) was also examined (●). Each symbol represents the mean value of three independent experiments ± S.E., and solid lines represent the fitted lines. The asterisks represent a statistically significant difference shown by Dunnett's test (*, $p < 0.05$; **, $p < 0.01$).

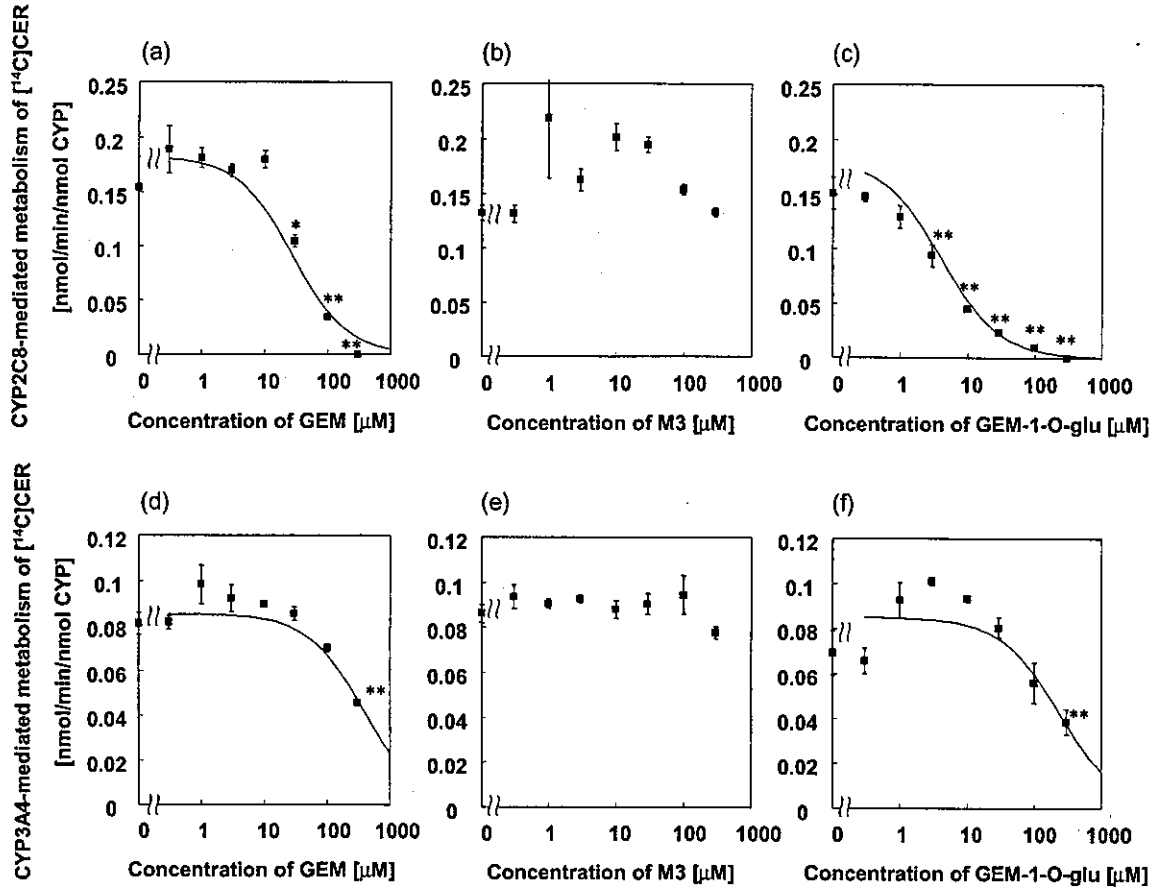

Fig. 3. Effect of GEM and its metabolites on the CYP2C8- and 3A4-mediated metabolism of [^{14}C]CER. Inhibitory effects of GEM (a, d), M3 (b, e), and GEM-1-*O*-glu (c, f) on the metabolism of [^{14}C]CER in CYP2C8 (a, b, c) and 3A4 (d, e, f) expression systems were examined. Each symbol represents the mean value of three independent experiments ± S.E., and solid lines represent the fitted lines. The asterisks represent a statistically significant difference by Dunnett's test (*, $p < 0.05$; **, $p < 0.01$).

was 37%, at most. In addition, 0.1 μM ketoconazole reduced M1 formation to 62.6 ± 5.6% (mean ± S.E.) of the control and slightly, but not significantly, reduced M23 formation to 77.6 ± 11.3% (mean ± S.E.) of the control (Fig. 6, e and f).

Inhibitory Effects of GEM and Its Metabolites on the in Vitro Metabolism of [^{14}C]CER in Pooled HLM. We examined the inhibitory effects of GEM and GEM-1-*O*-glu on the metabolism of [^{14}C]CER in pooled HLM (Fig. 7). GEM and GEM-1-*O*-glu inhibited the metabolism of [^{14}C]CER in pooled HLM in a concentration-dependent manner (Fig. 7), whereas M3 had no effects (data not shown). Figure 7 also shows simulation curves for the inhibitory effects of GEM and GEM-1-*O*-glu in pooled HLM based on eq. 3.

Human Serum Protein Binding of GEM and Its Metabolites. We examined the protein binding of GEM and its metabolites in 50 mM phosphate-buffered human serum (pH 7.4). The unbound fractions (f_u) of GEM, M3, and GEM-1-*O*-glu were 0.648 ± 0.037, 1.23 ± 0.00, 11.5 ± 2.3% (mean ± S.E.), respectively.

Discussion

It has already been reported that GEM is an inhibitor of P450- and UGT-mediated metabolism of CER (Prueksaritanont et al., 2002b,c; Wang et al., 2002). In the present study, we showed that GEM inhibited the OATP2-mediated uptake of CER as well as its metabolism (Fig. 2). The IC_{50} value of GEM for OATP2-mediated uptake of [^{14}C]CER (72 μM) was similar to, or lower than, the reported IC_{50} values for metabolism (Prueksaritanont et al., 2002b,c; Wang et al., 2002). We also found that a metabolite of GEM, GEM-1-*O*-glu, was a potent inhibitor of OATP2-mediated hepatic uptake of CER with a lower IC_{50} value (24 μM) than that of GEM itself (Fig. 2). This finding was matched by the fact that many glucuronides are recognized by OATP family transporters as substrates and/or inhibitors with a high affinity (König et al., 2000a,b, Cui et al., 2001).

We also examined the inhibitory effect of GEM and its metabolites on the CYP2C8- and 3A4-mediated metabolism of [^{14}C]CER. In the present TLC analysis, two clear bands for metabolites were detected in the experiment using the CYP2C8 expression system, whereas only one clear band for the metabolite was detected in the CYP3A4 experiment. Because Wang et al. (2002) reported that CYP2C8 and 3A4 equally catalyzed the formation of M1 although the formation rate of M23 was 14-fold lower in CYP3A4 than in CYP2C8, we identified these two bands as M1 and M23, respectively. The results of the inhibition studies should be discussed in relation to previous reports (Prueksaritanont et al., 2002c; Wang et al., 2002). Wang et al. (2002) reported that GEM inhibited CYP2C8-mediated metabolism of CER to M1 and M23 with IC_{50} values of 78 and 68 μM, respectively. The corresponding values in the present analysis were 37 and 30 μM, respectively (Fig. 4), and these are comparable

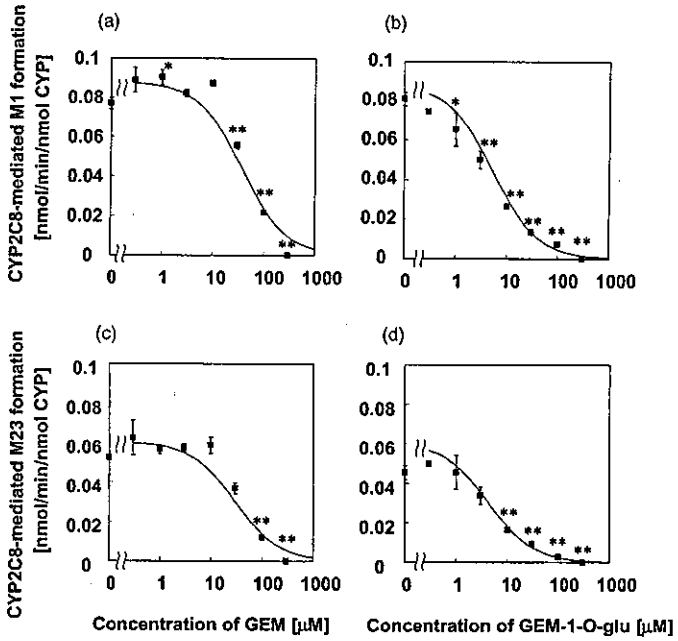

Fig. 4. Effect of GEM and GEM-1-*O*-glu on the CYP2C8-mediated M1 and M23 formation of [^{14}C]CER. Inhibitory effects of GEM (a, c) and GEM-1-*O*-glu (b, d) on the CYP2C8-mediated M1 formation (a, b) and M23 formation (c, d) were examined. Each symbol represents the mean value of three independent experiments ± S.E., and solid lines represent the fitted lines. The asterisks represent a statistically significant difference shown by Dunnett's test (*, $p < 0.05$; **, $p < 0.01$).

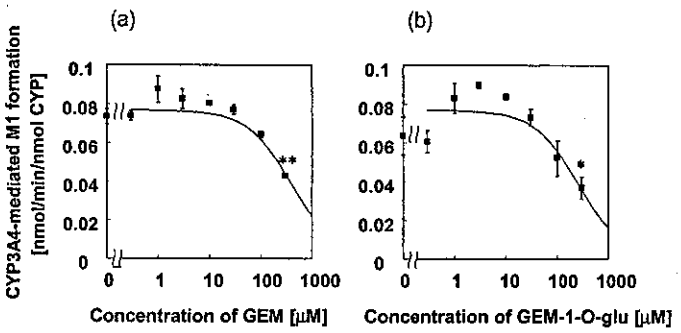

Fig. 5. Effect of GEM and GEM-1-*O*-glu on the CYP3A4-mediated M1 and M23 formation of [^{14}C]CER. Inhibitory effects of GEM (a) and GEM-1-*O*-glu (b) on the CYP3A4-mediated M1 formation were examined. Each symbol represents the mean value of three independent experiments ± S.E., and solid lines represent the fitted lines. The asterisks represent a statistically significant difference shown by Dunnett's test (*, $p < 0.05$; **, $p < 0.01$).

with the values reported by Wang et al. (2002). Prueksaritanont et al. (2002c) reported that the IC_{50} values of GEM for M1 and M23 formations in HLM were 220 and 87 μM, respectively, and Wang et al. (2002) reported the corresponding values to be >250 and 95 μM, respectively. As shown in Fig. 7, we also observed a concentration-dependent reduction in M1 and M23 formation in HLM. The apparent IC_{50} values of GEM for M1 and M23 formation in HLM was calculated to be 234 and 26 μM, respectively (Fig. 7), and these are also similar to results in previous reports (Prueksaritanont et al., 2002c; Wang et al., 2002).

Atypical effects of inhibitors were found in the present study, i.e., M3 apparently activated the CYP2C8-mediated metabolism of [^{14}C]CER at low concentrations, and GEM-1-*O*-glu activated the CYP3A4-mediated metabolism and M1

TABLE 1
IC_{50} values of GEM and GEM-1-*O*-glu on the OATP2-mediated uptake and metabolism of [^{14}C]CER[a]

	GEM	GEM-1-*O*-glu
	μM	
OATP2-mediated uptake	72.4 ± 28.4	24.3 ± 19.8
CYP2C8-mediated metabolism	28.0 ± 4.3	4.07 ± 1.23
CYP3A4-mediated metabolism	372 ± 100	243 ± 59

[a] All data are represented as the mean ± computer-calculated S.D.

formation at low concentrations, whereas it inhibited them at higher concentrations (Figs. 3 and 5), although these activations were not statistically significant with a few exceptions. These atypical effects of inhibitors may be explained by a multisite kinetic analysis involving a mixed effect of GEM and its metabolites as inhibitors and activators of enzymatic reactions (Galetin et al., 2002, 2003). However, in the present study, the enhancing effect was at most 1.5-fold, and this would have only a minimal effect on drug disposition in clinical situations, if any. Therefore, we analyzed the effects of GEM and its metabolites by a simple eq. 2.

In the present study, we showed that GEM and GEM-1-*O*-glu inhibited OATP2-mediated hepatic uptake and metabolism of [^{14}C]CER. Hence, the coadministration of GEM may lead to a DDI due to the inhibition of hepatic uptake and/or metabolism of CER. The possibility of a clinically relevant DDI should be discussed taking the therapeutic concentration of GEM and its metabolites into consideration because the intrinsic hepatic clearance will fall to $1/(1+ I/IC_{50})$ of control, where I is the inhibitor concentration (Ueda et al., 2001). In the report by Backman et al. (2002), the mean maximum concentration of GEM after repeated oral administration of 600 mg twice daily was 150 μM. Okerholm et al. (1976) measured the plasma concentrations of free GEM, its glucuronide conjugates, and other metabolites after a single oral administration of 600 mg of [^{3}H]GEM in normal human subjects receiving 600 mg of unlabeled GEM twice daily for 6 days and reported that the maximum concentration of glucuronide conjugates, mainly GEM-1-*O*-glu, was approximately 20 μM, whereas that of total GEM (GEM + glucuronide conjugate) was approximately 100 μM. Hengy and Kölle (1985) also reported that 10 to 15% of GEM in plasma was present as glucuronide conjugates. The reported values of the total concentrations of GEM and GEM-1-*O*-glu were similar or higher than the IC_{50} values for the metabolism and hepatic uptake of CER in the present study. However, because of the high plasma protein binding, the unbound concentrations of GEM and GEM-1-*O*-glu were at most 0.97 and 2.3 μM, respectively, i.e., less than the IC_{50} values obtained in the present study. Because only unbound drugs interact with transporters, this result suggests that it is unlikely to cause the reported serious DDI between CER and GEM. However, it is possible that GEM or its metabolites inhibit the metabolism of CER in the liver if they are actively transported to the liver and accumulate there. Indeed, Sallustio et al. (1996) have reported that GEM-1-*O*-glu is actively taken up by perfused rat liver and the liver/perfusate concentration ratio is 35 to 42. Assuming that it also accumulates in human liver, its unbound concentration there would be higher than the IC_{50} value for the microsomal metabolism, which gives a $1+ I/IC_{50}$ value of 3.1 to 3.2, i.e., more than a 3-fold reduction in the intrinsic hepatic clearance, suggesting that it may

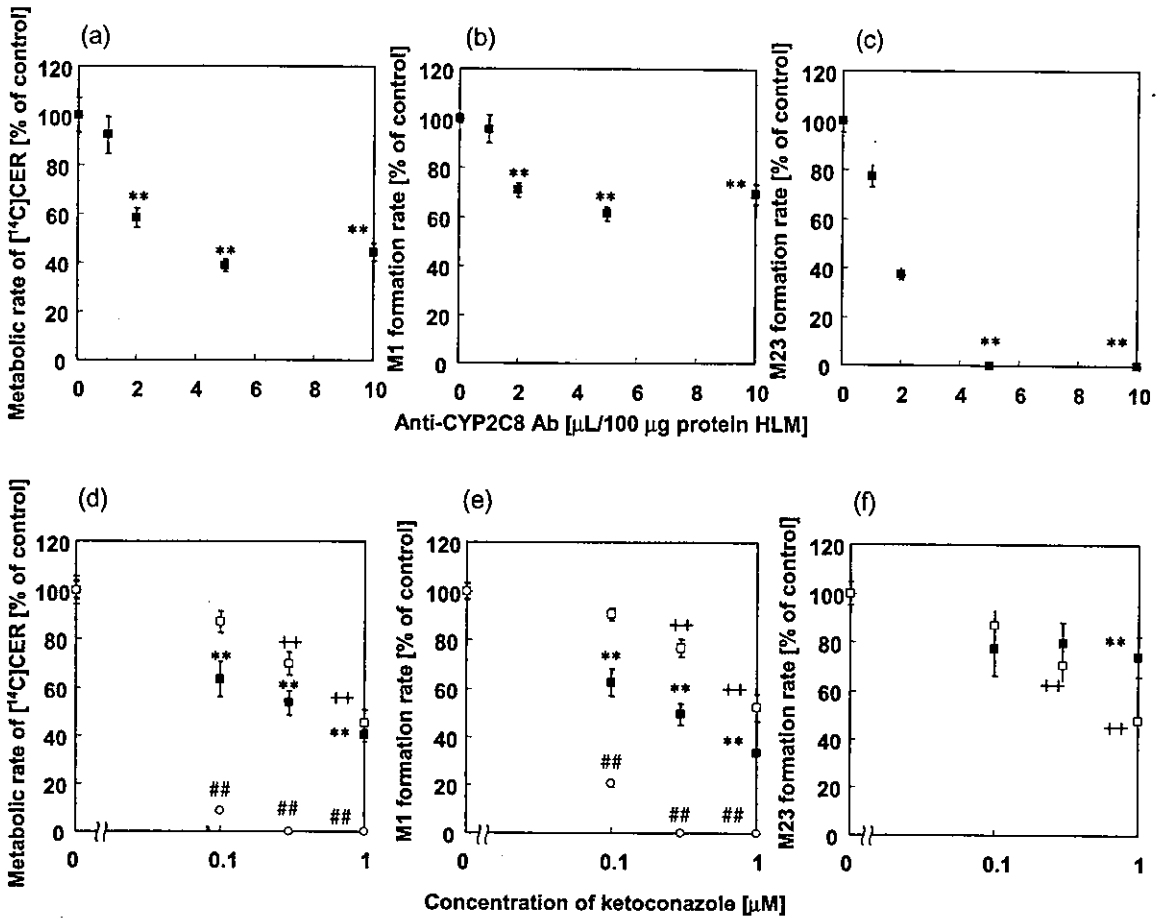

Fig. 6. Effect of specific inhibitory antibody against CYP2C8 (anti-CYP2C8 Ab) and ketoconazole on the metabolism of CER in HLM. The inhibitory effects of anti-CYP2C8 Ab (a) and ketoconazole, a potent CYP3A4 inhibitor (d), on the metabolism of [^{14}C]CER in pooled HLM (■) were examined. Their effects on M1 formation (b, e) and M23 formation (c, f) are also represented. The effect of ketoconazole on the metabolism of [^{14}C]CER in CYP2C8 (□) and CYP3A4 (○) expression systems was also examined. Each symbol represents the mean value of three independent experiments ± S.E., and solid lines represent the fitted lines. Symbols (*, +, and #) represent a statistically significant difference from the control values shown by Dunnett's test (*, $p < 0.05$; **, $p < 0.01$ for the metabolism in HLM; +, $p < 0.05$; ++, $p < 0.01$ for CYP2C8-mediated metabolism; and #, $p < 0.05$; ##, $p < 0.01$ for CYP3A4-mediated metabolism).

cause a serious DDI. In Table 2, the therapeutic total and unbound concentrations in the blood, the estimated unbound concentration in the liver, and the effects on the intrinsic hepatic clearances are summarized.

In the present study, GEM and GEM-1-*O*-glu preferentially inhibited CYP2C8-mediated metabolism of CER compared with CYP3A4-mediated metabolism (Figs. 3–5). These results support the findings by Backman et al. (2002) who reported that the AUC of M23 was markedly reduced to 17% of the control, whereas that of the open acid form of CER, the lactone form of CER, and M1 were 4.4, 3.5, and 3.5 times higher than the control. Because M23 formation is predominantly mediated by CYP2C8, and not by 3A4, the inhibition of CYP2C8 satisfactorily explains this DDI. In the report by Backman et al. (2002), all the AUC ratios for each of the metabolites to the open acid form of CER fell, following coadministration of GEM, to 82, 8.8, and 80% of the control for M1, M23, and the lactone form of CER, respectively. The slight reduction in the AUC of M1 and the lactone form may be partly due to GEM and GEM-1-*O*-glu inhibition of the hepatic uptake of CER, followed by M1 and M23 formation and lactonization in the liver.

Other statins, including simvastatin, lovastatin, pravastatin, and pitavastatin, are also affected by the coadministration of GEM (Backman et al., 2000, 2002; Kyrklund et al., 2001, 2003; Mathew et al., 2004). GEM increases the AUC of the open acid form of these statins (Backman et al., 2000, 2002; Kyrklund et al., 2001, 2003; Mathew et al., 2004). However, it does not affect the AUC of the lactone form of simvastatin and lovastatin and reduces that of pitavastatin (Backman et al., 2000; Kyrklund et al., 2001; Mathew et al., 2004), and it has no effect at all on the plasma concentration of fluvastatin (Spence et al., 1995). The limited effect of GEM only on the plasma concentrations of the open acid forms of simvastatin and lovastatin can be explained by inhibition of lactone formation followed by UGT-mediated glucuronidation (Prueksaritanont et al., 2002c). The reduced AUC of the lactone form of pitavastatin may also be explained by the same mechanism (Fujino et al., 2003). On the other hand, the increase in the AUC of the open acid forms of pravastatin and pitavastatin may be partly explained by minor inhibition of their OATP2-mediated uptake (Table 2), because these statins are substrates of OATP2 (Hsiang et al., 1999; Nakai et al., 2001; Hirano et al., 2004). GEM increases the AUC of pravastatin and pitavastatin only by 2.0- and 1.5-fold, respectively, whereas it increases that of CER 4.4-fold (Backman et al., 2002; Kyrklund et al., 2003; Mathew et al., 2004). The increase in the AUC of pravastatin can be partly ex-

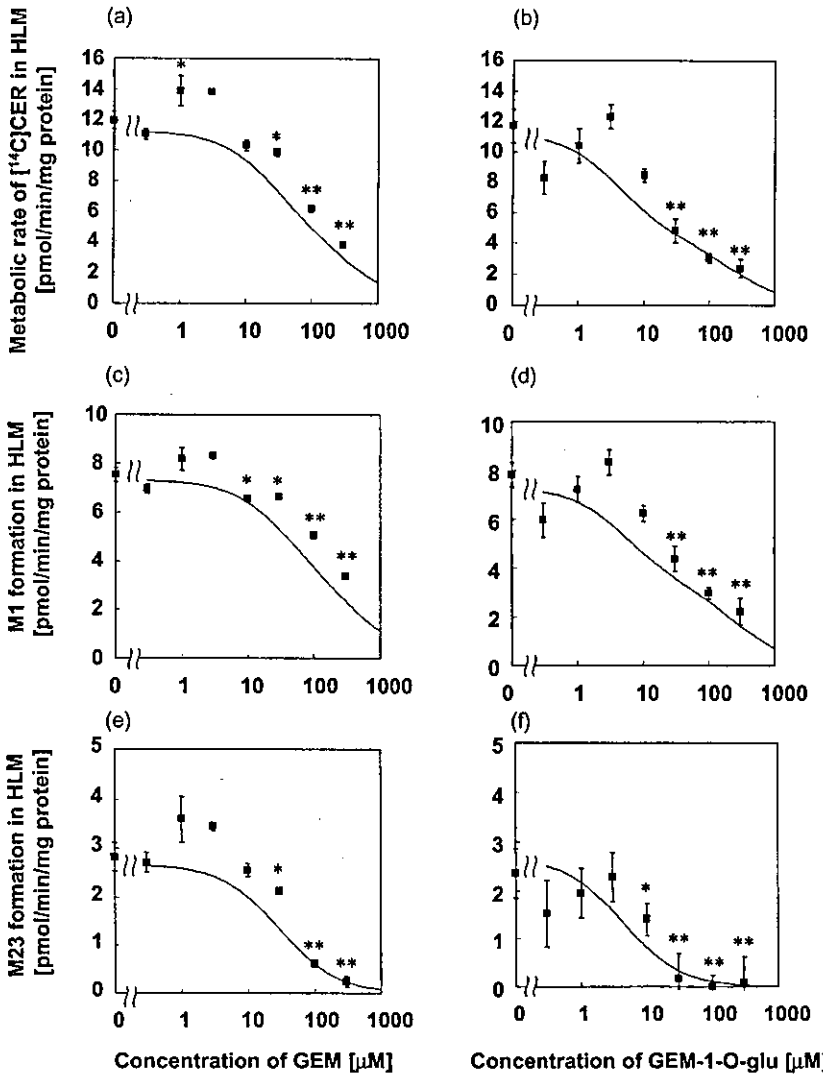

Fig. 7. Effect of GEM and its metabolites on the metabolism of [^{14}C]CER in HLM. The inhibitory effects of GEM (a, c, e) and GEM-1-*O*-glu (b, d, f) on the metabolism of [^{14}C]CER (a, b) and the formation of M1 (c, d) and M23 (e, f) in pooled HLM were examined. Each symbol represents the mean value of three independent experiments ± S.E. Solid lines represent simulated lines based on eq. 3. The asterisks represent a statistically significant difference shown by Dunnett's test (*, $p < 0.05$; **, $p < 0.01$).

TABLE 2
Plasma and liver concentrations of GEM and its metabolites and their estimated inhibitory effects on the elimination of CER in the liver in clinical situations[a]

	GEM	GEM-1-*O*-glu
C_{max}[b] (μM)	100–150	20
$1+I/IC_{50,OATP2}$	2.4–3.1	1.8
$1+I/IC_{50,metabolism}$	2.2–2.6	2.2
$C_{max,u}$[c] (μM)	0.65–0.97	2.3
$1+I/IC_{50,OATP2}$	1.0	1.1
$1+I/IC_{50,metabolism}$	1.0	1.3
$C_{max,u,liver}$[d] (μM)		81–97
$1+I/IC_{50,metabolism}$		3.1–3.2

[a] Inhibitory effects of GEM and GEM-1-*O*-glu are represented by 1 + inhibitor concentration (I)/IC_{50}.
[b] Plasma concentrations of GEM and GEM-1-*O*-glu are reported by Backman et al. (2002) and Okerholm et al. (1976).
[c] Plasma unbound concentrations.
[d] Estimated unbound concentrations in the liver.

plained by its reduced renal excretion, and therefore, the effect of GEM on its elimination in the liver is weaker (Kyrklund et al., 2003). On the other hand, cyclosporin A, an inhibitor of OATP2, markedly increases the AUC of pravastatin and pitavastatin as well as CER (Regazzi et al., 1993; Hasunuma et al., 2003). The variety of effects on different statins may be due to the fact that GEM and its metabolites inhibit both the uptake and CYP2C8-mediated metabolism of CER in the liver, whereas they inhibit only the hepatic uptake of pravastatin and pitavastatin to a small extent (Table 2); on the other hand, cyclosporin A inhibits their hepatic uptake at therapeutic concentrations (Shitara et al., 2003).

In conclusion, we have shown that GEM moderately inhibits, whereas GEM-1-*O*-glu potently inhibits, the CYP2C8-mediated metabolism, and both moderately inhibit the OATP2-mediated hepatic uptake of drugs. Their inhibition of the CYP2C8-mediated metabolism of CER (mainly by GEM-1-*O*-glu concentrated in the liver) is a major mechanism that governs the clinically relevant DDI between CER and GEM, whereas their inhibition of the OATP2-mediated hepatic uptake of CER may also contribute to the DDI but to a lesser extent.

Acknowledgments

We are grateful for Bayer AG and Bayer Yakuhin for kindly providing the radiolabeled and unlabeled CER. We are also grateful for Sankyo Co., Ltd. (Tokyo, Japan) and Chemtech Labo. Inc. (Tokyo, Japan) for providing GEM-1-*O*-glu. We appreciate the generosity of Pharsight Corporation for providing a license for the computer program, WinNonlin, as part of the Pharsight Academic License (PAL) program.